

FILE COPY  
NO 3

RM L50A31



# RESEARCH MEMORANDUM

WING-FLOW MEASUREMENTS OF LONGITUDINAL STABILITY AND  
CONTROL CHARACTERISTICS OF A CANARD AIRPLANE  
CONFIGURATION WITH A 45° SWEPTBACK WING AND  
A TRIANGULAR ALL-MOVABLE CONTROL SURFACE

By Harold L. Crane and James J. Adams

Langley Aeronautical Laboratory THIS DOCUMENT IS FROM THE FILES OF  
Langley Air Force Base, Va.

NATIONAL ADVISORY COMMITTEE FOR AERONAUTICS  
LANGLEY AERONAUTICAL LABORATORY  
LANGLEY FIELD, HAMPTON, VIRGINIA

RETURN TO THE ABOVE ADDRESSEE  
REQUESTS FOR PUBLICATIONS SHOULD BE ADDRESSED  
AS FOLLOWS:

NATIONAL ADVISORY COMMITTEE FOR AERONAUTICS  
1512 H STREET, N. W.  
WASHINGTON 25, D. C.

**NATIONAL ADVISORY COMMITTEE  
FOR AERONAUTICS**  
WASHINGTON

August 25, 1950  
Declassified August 23, 1954

NATIONAL ADVISORY COMMITTEE FOR AERONAUTICS

RESEARCH MEMORANDUM

WING-FLOW MEASUREMENTS OF LONGITUDINAL STABILITY AND  
CONTROL CHARACTERISTICS OF A CANARD AIRPLANE  
CONFIGURATION WITH A  $45^{\circ}$  SWEPTBACK WING AND  
A TRIANGULAR ALL-MOVABLE CONTROL SURFACE

By Harold L. Crane and James J. Adams

SUMMARY

Measurements of the longitudinal stability and control characteristics of a canard airplane configuration have been made by the wing-flow method. The distinguishing features of this configuration in addition to the unconventional wing-stabilizer arrangement are the triangular plan form of the all-movable longitudinal control surface, the  $45^{\circ}$  sweptback wing of aspect ratio 4.1, and the slender body of fineness ratio 13.5. The investigation included measurements of lift, pitching moment, and rolling moment of the semispan model, with control settings between  $-40^{\circ}$  and  $16^{\circ}$  and with the control surface removed. In some cases the angle-of-attack range was as great as from approximately  $-10^{\circ}$  to  $30^{\circ}$ . Approximate measurements of chord force were made at one stabilizer incidence. The Mach number range covered was from 0.55 to 1.14 at Reynolds numbers of the order of 400,000.

The transonic longitudinal stability and control characteristics of the test configuration at low or moderate lift coefficients were found to be exceptionally good. The stabilizing aerodynamic-center shift with increasing Mach number was small and its effect on the control deflections required for maneuvering was more than counteracted by the gradual increase in control effectiveness with increasing Mach number. At high lift coefficients an unstable pitching tendency developed due to loss in lift over the outboard portion of the wing. Use of a different airfoil section and stall-control devices to postpone the loss in lift would be highly desirable. The results indicate that the unstable pitching tendency can be avoided at some sacrifice of maximum lift by locating the center of gravity sufficiently far forward to cause the control surface to stall before the wing tip. These results, however, do not indicate what the dynamic behavior of the configuration would be at the stall, and further investigation would be required to determine possible adverse effects of this remedy on the control characteristics at the stall.

The experimental data obtained are presented in a summarized or abridged form. In addition, calculated trim curves are presented for various flight loading conditions. The expressions developed for convenient calculation of trim curves from the wing-flow data are also presented. Some discussion of the effects of aeroelastic deformation in the form of wing bending along the span is included. Comparisons are made with unpublished force-test data from the Langley free-flight tunnel and with wing-flow data for two transonic configurations with conventional tail locations. In general, the wing-flow data obtained at subcritical Mach numbers were in agreement with the wind-tunnel data.

#### INTRODUCTION

An experimental investigation of the longitudinal stability and control characteristics at transonic speeds of the tail-first or canard-type airplane is being conducted at the Langley Laboratory. This investigation was undertaken after a theoretical study (reference 1) indicated that it might be possible to design a canard which has desirable transonic stability and control characteristics compared to tail-aft configurations and also has acceptable characteristics at low speeds. The tests reported herein were made by the NACA wing-flow method on a 3.15-inch semispan model having an untapered  $45^\circ$  sweptback wing of aspect ratio 4.1, a 0.90-inch semispan  $60^\circ$  delta-shaped control surface, and a fineness ratio 13.5 body of circular cross section. This model was an 0.075-scale version of a free-fall model. Reference 2 presents the results of the canard free-fall test program. The considerations which resulted in the selection of the particular components of the test configuration are also discussed in reference 2.

The Mach numbers at which the wing-flow tests were made ranged from 0.55 to 1.14 and the Reynolds number varied from approximately 225,000 to 570,000. Lift and pitching moment about an axis 40 percent chord ahead of the mean aerodynamic chord (-40 percent  $\bar{c}$ ) were measured through an angle-of-attack range of approximately  $-10^\circ$  to  $12^\circ$  with control-surface incidence settings of  $-3.8^\circ$ ,  $1.8^\circ$ ,  $5.8^\circ$ ,  $11.2^\circ$ , and  $15.8^\circ$ . Rolling moment about the body axis of the half-span model, pitching moment, and lift were measured with the horizontal control surface removed. Normal force, pitching moment, and chord force were measured for angles of attack from  $-10^\circ$  to  $30^\circ$  with the horizontal control surface at  $1.8^\circ$  incidence.

Not all the data obtained are presented in this paper. Only the minimum number of plots necessary to give the essence of the data obtained are included. For a comparison of results, unpublished data from the force tests of this canard configuration in the Langley free-flight tunnel and also some data obtained from wing-flow tests of two other transonic

configurations with conventional tail locations are included. A list of definitions of the symbols used in presenting the data is given in appendix I.

#### APPARATUS

The configuration tested consisted of a  $45^{\circ}$  sweptback wing mounted behind the maximum diameter of a fineness-ratio-13.5 fuselage with a  $60^{\circ}$  delta-shaped all-movable control surface at the nose. The untapered wing had a semispan of 3.15 inches, an aspect ratio of 4.1, and an NACA 65-009 airfoil section perpendicular to the leading edge. The incidence of the control surface, which had a 0.90-inch semispan and a thin flat-sided cross section, was varied by rotation about a line through 63 percent of the root chord. Figure 1 shows the configuration and dimensions of the model.

Wing and control surface were fabricated from solid duralumin. The fuselage was of mahogany reinforced with duralumin. A spring-steel end plate was attached to the model to act as a reflection plane and to isolate the model from irregular air flows originating at the support slot in the test panel. The center-line plane along which the model was divided was bent to the shape of the test panel so as to conform to the air flow.

The model was mounted on the ammunition door of an F-51D airplane. The contour of the door has been modified to reduce the velocity gradient across the door and to place the wing shock wave behind the model. A photograph of the canard model in place on the test panel is presented in figure 2, and plots of the velocity gradients are shown in figure 3. The average Mach number over the model wing was determined from the pressure-distribution data obtained in preliminary investigations of the flow over the door, and was plotted for use in data reduction as a function of Mach number and lift coefficient of the F-51D test airplane. The results presented herein are plotted in terms of the average Mach number of the flow over the model wing.

Two balances were used in the test program. One of these was a strain-gage balance which measured rolling moment about the body axis, lift and pitching moment; and which could operate in an angle-of-attack range of  $-10^{\circ}$  to  $12^{\circ}$ . The other balance was a deflection type linked to an autosyn system which measured normal force, pitching moment, and chord force, and which could operate over any preset angle-of-attack range of  $10^{\circ}$  between  $-10^{\circ}$  and  $30^{\circ}$ . This balance is hereinafter referred to as the autosyn balance. With either balance an electric motor was used to

oscillate the model at a rate of angle-of-attack change of approximately one radian per second or slower. This rate of oscillation resulted in angle-of-attack change of  $1^{\circ}$  or less per 100 chord lengths of motion.

The impact and static pressure, free-air temperature, and normal acceleration for the flight condition of the F-51D test airplane were measured with standard NACA instruments. One other measurement required was the correction for the angle of attack necessitated by the fact that small amounts of yaw were usually present in the flow at the test location. A wedge-shaped vane located 22 inches outboard of the model and calibrated to measure the angle of flow at the model location was used for this purpose.

The following test flights were made:

Flight	Control-surface setting, (deg)	Angle-of-attack range, (deg)	Balance
1	Off	-10 to 12	Strain gage
2	1.8	-10 to 12	Do.
3	5.9	-10 to 12	Do.
4	11.2	-10 to 12	Do.
5	15.8	-10 to 12	Do.
6	-3.8	-10 to 12	Do.
7	Off	-10 to 12	Do.
8	1.8	-10 to 0	Autosyn
9	1.8	0 to 10	Do.
10	1.8	10 to 20	Do.
11	1.8	20 to 30	Do.

Each flight consisted of two or more runs made at different altitudes in order to obtain a spread in Reynolds number. A high dive from 28,000 feet to 21,000 feet and a low dive from 18,000 feet to 12,000 feet were made. Also included in the paper are data obtained from one level-flight run made at 5,000 feet. A plot of Reynolds number against Mach number for the various runs is shown in figure 4.

#### PRECISION OF MEASUREMENTS

A sample of the galvanometer record from the strain-gage balance is shown in figure 5. An example of the data obtained from such records showing the scatter of the test points is presented in figure 6. The variations of normal-force coefficient, pitching-moment coefficient, and

chord-force coefficient with angle of attack are shown at a Mach number of 1.0 for the complete canard model with the control surface set at  $1.8^\circ$  incidence. Above  $10^\circ$  angle of attack the spread in the test points is comparatively large. This increased spread resulted chiefly from the necessity for reducing the rate of oscillation of the balance in the high angle-of-attack range to circumvent mechanical difficulties which had developed in the balance. The decreased rate of oscillation caused the change in Mach number and dynamic pressure over a given angular cycle to be about twice as large as had been the case for the tests at angle of attack less than  $10^\circ$ . The spread was particularly noticeable in data for a Mach number of 1.0 because the most rapid changes in lift and moment characteristics with Mach number occurred between  $M = 0.95$  and  $M = 1.0$ . However, the quality of the data was considered to be good enough to illustrate the approximate variations of the measured parameters at high angles of attack.

An estimation of the accuracy of the various measurements is presented in the following table:

Variable	Approximate possible error		
	In absolute value	In coefficient	
		$q = 200 \text{ lb/sq ft}$	$q = 800 \text{ lb/sq ft}$
Mach number, $M$ , percent . . .	$\pm 2$	-----	-----
Dynamic pressure, $q$ , percent . . . . .	2	-----	-----
Angle of attack, $\alpha$ , deg . . .	.5	-----	-----
Tail incidence, $it$ , deg . . .	.5	-----	-----
Normal force, $N$ , or Lift, $L$ , lb . . . . .	.5	$\pm 0.08$	$\pm 0.02$
Chord force, $C$ , lb . . . .	.2	.04	.01
Pitching moment, $M$ , in-lb . .	.8	.08	.02
Rolling moment, $L'$ , in-lb . .	.5	.02	.005

Approximate possible errors in the values of measured quantities and in the coefficients of force and moment are presented. The approximate possible errors in the coefficients tend to vary inversely with dynamic pressure and are presented in the foregoing table for the minimum and maximum dynamic pressures. The values of possible errors presented do not take into account the effects of the velocity gradient over the model. No correction was made for the effect of the end plate on the chord force. It should be noted that errors in increments of any measured variable determined from the faired curves presented herein will be considerably smaller than errors in absolute values.

## RESULTS AND DISCUSSION

Data Presentation and General Discussion  
of Mach Number Effects

The variations of normal-force, chord-force, and pitching-moment coefficients with angle of attack are presented in figure 7 for the complete model with the control surface set at  $1.8^\circ$ . Lift, pitching-moment, and rolling-moment coefficients with control surface removed are plotted as a function of angle of attack in figure 8. As stated in the section entitled "Apparatus," two balances were used during this test program, one of which measured normal force while the other measured lift. However, the calculated difference between normal-force coefficient and lift coefficient was within the accuracy of the data in the range of angles of attack presented in figure 8. The data are presented for increments of Mach number of 0.05 or 0.10 throughout the test range for the two Reynolds number ranges.

Examination of these data showed that the effects of Mach number on the measured parameters were small and gradual. There was little change with Mach number in the variation of normal-force coefficient, pitching-moment coefficient, or rolling-moment coefficient with angle of attack for angles of attack below  $10^\circ$ . The variation of normal-force coefficient with angle of attack tended to remain linear to higher angles of attack at the higher test Mach numbers. The effect of Mach number on the variation of pitching-moment coefficient with angle of attack beyond  $10^\circ$  angle of attack was not clearly defined, but appeared to be small.

Figure 9 presents the variation of pitching-moment coefficient with angle of attack at a Mach number of 0.9 for various control-surface incidence settings. The variation of pitching-moment coefficient per degree of control deflection with Mach number was determined from plots similar to figure 9 and is presented in figure 10. The control effectiveness varied gradually with Mach number, increasing approximately one-third as the Mach number increased from 0.6 to 1.1. It was found that the control effectiveness was roughly constant with angle of attack as long as the sum of the angle of attack and the control incidence did not exceed  $25^\circ$ .

Lift-drag polars calculated from the normal-force and chord-force data are presented in figure 11. These data should not be considered to be very accurate because of the fact that no correction for end-plate drag has been applied and because past experience indicates that wing-flow-drag results, particularly on half-models of fuselages, are usually too high.

An attempt was made to compare the drag results with experimental or theoretical values from other sources. The variation of drag coefficient at zero lift with Mach number for the same configuration at over 20 times the Reynolds number of the wing-flow tests was available from reference 2. A comparison with these results indicated that zero-lift drag coefficients measured by the wing-flow method were high by a factor of approximately three. An estimate of the subsonic variation of induced drag with lift coefficient was made by using the experimental data of reference 3 as a measure of the drag of the control surface and determining the induced drag of the wing from the theory for an elliptical lift distribution. Again the wing-flow results proved to be high. The rate of change of induced drag with the square of the lift coefficient

$\frac{C_{Di}}{C_L^2}$  appeared to be high by a factor of two. It is still possible

that the trends indicated by the wing-flow results for the effects of Mach number on induced drag or drag due to lift were qualitatively correct. These effects can be summed up by the statement that for

moderate lift coefficients the parameter  $\frac{C_{Di}}{C_L^2}$  was nearly constant over

the test range of Mach numbers.

#### Stability at Small Angles of Attack

The variations of normal-force and pitching-moment coefficient with angle of attack (figs. 7 and 8) were approximately linear for small angles of attack. The variations with Mach number of the stability parameters,  $C_{L\alpha}$  the rate of change of lift coefficient with angle of attack,  $C_{m\alpha}$  the

rate of change of pitching-moment coefficient with angle of attack, and  $C_{l\alpha}$  the rate of change of rolling-moment coefficient of the semi-

span model with angle of attack, at  $0^\circ$  angle of attack are shown in figure 12. The values of these parameters all tend to increase gradually with increasing Mach number up to approximately  $M = 0.95$  beyond which they decrease with increasing Mach number. The ratio of the slopes  $C_{m\alpha}$  and  $C_{N\alpha}$  also presented in figure 12 is a measure of the control-fixed longitudinal stability for maneuvers at constant speed. The maneuver point or aerodynamic-center position was approximately 30 percent chord ahead of the leading edge of the mean aerodynamic chord at a Mach number of 0.55 and moved rearward approximately 15 percent chord as the Mach number increased to 1.0. Above this Mach number the maneuver point again moved forward. The maneuver-point shift with Mach number for this canard configuration has approximately the same magnitude as the smallest shift so far measured with a conventional configuration. In figure 12 it appears that the aerodynamic-center position is considerably affected by

Reynolds number (scale effect). However, because the magnitude of the aerodynamic-center shift between the two runs was approximately proportional to the dynamic pressure, wing flexibility was investigated as a possible cause for these differences.

Calculations of aeroelastic distortion were made considering that the wing bent as a cantilever beam. Because the wing was swept back, this type of bending would cause a progressive change in angle of attack along the span of the wing. Approximately the same results were obtained when a uniform load distribution was assumed and when the root section was assumed to be loaded twice as heavily as the tip section with a linear variation in between. These calculations indicated that the angle of attack of the tip section would be reduced a maximum of 50 percent under the most severe test loading encountered. An experimental check by static loading indicated that the results of the deflection calculations for the assumed loadings were approximately correct.

The effect of wing bending on the chordwise aerodynamic-center position of the  $45^{\circ}$  sweptback wing is shown in figure 13. The maximum calculated aerodynamic-center shift for the wing due to flexibility was of the order of 10 percent chord. Because the lift-curve slope of the wing would be reduced by wing bending while it was assumed that the low-aspect-ratio control surface was rigid, the calculated aerodynamic-center shift of the complete configuration, which is also shown in figure 13, was approximately twice as large as for the wing alone. The effect of wing flexibility on the aerodynamic-center position of a canard configuration can be reduced by increasing the flexibility of the tail surface relative to that of the wing. The data of figure 13 indicate that the larger part of the effect of Reynolds number on the data presented herein may have been due to aeroelastic distortion rather than to scale effect.

The chordwise and spanwise aerodynamic-center shifts of a  $45^{\circ}$  sweptback wing due to bending should be nearly equal. Therefore, it seemed that the spanwise center-of-lift locations of the semispan model determined from the tail-off rolling-moment data of figure 8 could be used as a check on the results of the flexibility calculations. This determination indicated that the center of lift of the canard wing at small angles of attack was slightly inboard of the midsemispan point. It could be concluded that the effect of Mach number on the lateral center of pressure of the wing panel was small. However, the scatter in the results ( $\pm 2$  percent semispan) was sufficient to mask any effect of Reynolds number (dynamic pressure) of the order of magnitude predicted by the flexibility calculations on the spanwise center-of-lift location.

## Stability at Large Angles of Attack

As has been stated, the slope of the lift or normal-force curve at any Mach number was relatively constant up to an angle of attack of approximately  $10^\circ$ . (See figs. 7 and 8.) For angles of attack greater than  $10^\circ$  the rate of change of normal-force coefficient with angle of attack decreased considerably, but further increases in normal force with increasing angle of attack occurred up to  $30^\circ$ , the maximum of the present tests. That the first loss in lift occurred at the wing tip was apparent from the determination of the approximate spanwise center of lift using the rolling-moment data of figure 8 which showed that the center of lift moved inboard perhaps 5 to 8 percent of the semispan below  $12^\circ$  angle of attack. This tendency can also be seen in the galvanometer record shown in figure 5. At the largest test angles of attack the slope of the normal-force curve began to increase. One possible explanation for the reflex in the normal-force curves is that at very large angles of attack the component of the drag in the direction of the normal-force coefficient becomes increasingly large.

It should be noted that at full-scale Reynolds numbers the initial break in the normal-force curves would probably occur at an angle of attack somewhat larger than  $10^\circ$ . It should also be noted that at the higher angles of attack the variation of normal-force coefficient does not accurately reflect the variation of lift coefficient with angle of attack. However, the variation of normal-force coefficient with angle of attack can be used directly in calculations of longitudinal stability throughout the angle-of-attack range.

The quality of the pitching-moment data was not sufficiently high to accurately define small stability changes. Therefore, in the analysis of the data obtained the variation of pitching-moment coefficient with angle of attack was considered to be approximately linear for angles of attack less than  $10^\circ$ . With a tail deflection of  $1.8^\circ$ , a large unstable break in the moment curve occurred at approximately  $10^\circ$ . (See figs. 8(c) and 8(d).) The unstable moment variation was evidently partly a result of tip stalling and largely a result of more general loss in lift-producing effectiveness of the wing. The unstable moment break can be delayed to larger angles of attack by means of properly designed stall-control devices. (Reference 4 presents the results of an investigation of such devices on a  $42^\circ$  sweptback wing.) It should be noted that, with center-of-gravity locations forward of the test location, stalling of any portion of the wing would cause a decrease in stability.

At an angle of attack of approximately  $20^\circ$  the pitching-moment curves break again, this time in the stable direction. It is believed that the stable moment break was caused by stalling of the control surface. In this case the incidence of the control surface was  $1.8^\circ$ . The angle of attack at which the stable moment break occurred would depend on the

incidence or deflection of the control surface. At a given Mach number, therefore, the angle of attack for the occurrence of the stable moment break would be dependent on the trim requirements and be affected by such variables as wing loading and center-of-gravity position. For forward center-of-gravity positions where the tail deflections required for trim would be large, the stable moment break due to tail stalling may occur at the same time or before the unstable moment break due to wing stalling and thereby eliminate the unstable variation of pitching moment with angle of attack in the range shown by the test data. Such a condition is indicated in figure 9 by the pitching-moment curve for a  $15.8^\circ$  tail setting.

#### Longitudinal Trim Characteristics

An expression has been derived for calculation of the longitudinal trim characteristics of the canard configuration. The derivation of this expression is discussed in appendix II. The calculated trim characteristics are for a configuration having the same flexibility as the model. The solid duralumin airfoil surfaces of the model were probably at least as rigid as the surfaces of a full-scale canard airplane would be. The variation of control-surface incidence required for longitudinal trim with trimmed lift coefficient is presented in figure 14 for two center-of-gravity positions for various Mach numbers for both ranges of test Reynolds numbers. These curves are based on the assumption that the control-effectiveness parameter  $C_{mit}$  is constant.

This assumption is reasonably correct for angles of flow with respect to the control surface up to approximately  $25^\circ$ , and the curves of figure 14(b) are presented only up to the point where the angle of flow with respect to the control surface exceeds  $25^\circ$ . The data of figure 14 indicate that the longitudinal stability as measured by the rate of change of control incidence with trimmed lift coefficient was reasonably constant up to lift coefficients of 0.6 to 0.8. The data of figure 14 show that with the center of gravity at -40 percent  $\bar{c}$  the canard configuration tested became unstable at trimmed lift coefficients of 0.6 to 0.8 at any Mach number in the test range. However, with the center of gravity at -80 percent  $\bar{c}$  large enough control-surface deflections would be required that loss of control effectiveness would occur at lift coefficients of 0.5 to 0.6 and would cause an effective increase in stability. At higher lift coefficients the rate of change of control deflection with trimmed lift coefficients would increase progressively until the control lost all effectiveness. The data of figure 9 for a control deflection of  $15.8^\circ$  indicate that the stall progression over the control surface was abrupt.

In order to assure that a canard configuration will have a nosing down tendency at the stall, it may be necessary for the control surface

to stall before the wing and as a result there must be some sacrifice in maximum lift. This loss in maximum lift is not necessarily greater than occurs with a tail-aft airplane configuration due to the incremental download produced by the control surface. To obtain as high maximum lift as possible with a nosing down tendency at the stall the center of gravity can be located somewhat behind -80 percent  $\bar{c}$ . However, it must be kept in mind that a nosing-down tendency produced by stalling of the control surface might produce undesirable dynamic characteristics. The use of properly designed stall-control devices on the wing to delay the unstable pitching-moment break and possibly to decrease the magnitude of the break will make it possible to locate the center of gravity farther back and thus to further increase the usable maximum lift coefficient.

The variation with Mach number of the parameter  $\delta_{it}/\delta C_L$  determined at low lift coefficients is presented in figure 15 for the canard configuration and for two conventional airplanes with  $35^\circ$  sweptback wings designed for flight at near sonic speeds. It should be noted that all three configurations were stable throughout the Mach number range. The ratio of maximum and minimum values of  $\delta_{it}/\delta C_L$  over the test Mach number range for the canard was about the same as for configuration 1 and was much less than that of configuration 2.

Increasing Reynolds number caused a small reduction in the rate of change of control-surface incidence with trimmed lift coefficient for the canard model. Approximate calculations, which have already been discussed, indicated that aeroelastic distortion would be of sufficient magnitude to account for a large part of the changes which appear from figures 14 and 15 to be due to Reynolds number (scale effect).

The variation of control incidence for trim with Mach number is presented in figure 16. This figure includes three plots which show the trim curves for two center-of-gravity positions, two altitudes, and two Reynolds number ranges at  $1g$  and  $4g$ . The data of figure 16 indicate that the trim changes with Mach number for trimmed lift coefficients which correspond to flight at  $1g$  were unusually mild for the test canard configuration. It is evident from the present investigation that the desirable trim characteristics at  $1g$  were largely a result of the following favorable conditions: The configuration was symmetrical with respect to the horizontal plane; the variation of aerodynamic-center position with Mach number was small; the control effectiveness increased gradually with increasing Mach number. However, with the rear center-of-gravity position, -40 percent  $\bar{c}$ , the canard would be subject to an unstable variation of control deflection with normal acceleration in maneuvers. For an acceleration of  $4g$  and an altitude of 40,000 feet the instability was present at all but the highest test Mach numbers. With the more forward center-of-gravity position considered, -80 percent  $\bar{c}$ , and for the conditions of the example presented in figure 16(a) stalling of the control surface eliminated the instability, but also restricted the maneuverability. The restriction would probably not be quite so severe

at full-scale Reynolds numbers as is indicated by these data in that the loss in lifting effectiveness of the wing would probably be delayed to higher angles of attack. In either case the optimum center-of-gravity position would be between the two which have been considered.

The use of stall-control devices to increase the range of operating lift coefficients while maintaining longitudinal stability may be possible at landing speeds, but would certainly become more difficult at high Mach numbers. However, as indicated by the data of reference 5, the shape of the lift curve which has a large effect on the stability of a canard is dependent on the airfoil section. The wing of the test configuration began to lose lifting effectiveness at an angle of attack of approximately  $10^\circ$  which corresponds to a lift coefficient of 0.6 or slightly higher. It is likely that, by changing the airfoil section of the test configuration to a section with which the lift curve of a sweptback wing was linear to higher angles of attack, a major improvement in the stability could be accomplished. The maneuverability with stick-fixed stability of the canard configuration under consideration would be increased accordingly.

#### Comparison with Low-Speed Wind-Tunnel Data

The wing-flow data have been compared with unpublished data from force tests in the Langley free-flight tunnel. Figure 17 shows that the variation of lift coefficient with angle of attack at  $M = 0.65$  was approximately the same as the free-flight-tunnel data for angles of attack up to  $10^\circ$  or  $12^\circ$ . The variation of pitching-moment coefficient with angle of attack for  $M = 0.65$  was very similar to that obtained from the free-flight-tunnel data throughout the angle-of-attack range. The two investigations were run at approximately the same Reynolds number,  $2.2 \times 10^5$  for the wing-flow tests and  $3.0 \times 10^5$  for the free-flight-tunnel tests. The Mach number for the free-flight-tunnel tests was about 0.05. The value of the stabilizer effectiveness parameter  $C_{mit}$  was determined to be approximately 0.018 by the free-flight-tunnel investigation. This value is in approximate agreement with the value of 0.015 obtained at the lowest test Mach number of the wing-flow investigation. The aerodynamic-center position was determined to be at -33 percent  $\bar{c}$  by the free-flight-tunnel investigation. This value compares favorably with the value of approximately -30 percent obtained at  $M = 0.55$  from the wing-flow tests. The wing-flow data showed approximately 25 percent larger aerodynamic-center shift due to addition of the tail than did the Langley free-flight-tunnel data.

## CONCLUSIONS

From the results of an investigation of the longitudinal stability and control characteristics of a canard airplane configuration by the wing-flow method, the following conclusions may be drawn:

1. A desirable feature of the test configuration was the small movement of aerodynamic-center position with increasing Mach number. The extreme movement of the aerodynamic-center position or of the control-fixed neutral point for constant-speed maneuvers measured was a rearward shift of 15 percent chord. The control effectiveness as indicated by the parameter  $C_{mit}$  gradually increased by approximately one-third as the Mach number increased from 0.6 to 1.1. Because the canard configuration was symmetrical, no change in trim at zero lift occurred. The increasing control effectiveness more than offset the effect of the small movement of the aerodynamic center with the result that the variation of control position for trim in level flight with Mach number was very desirable. The variation of stabilizer position with trimmed lift coefficient was approximately linear for moderate lift coefficients and was not greatly affected by variation of Mach number in the test range.
2. The wing of the test configuration was subject to loss in lift over the outboard portion of the wing at angles of attack greater than  $10^{\circ}$ . When this wing stall was encountered at small control deflections, an unstable pitching tendency resulted. At large control deflections (corresponding to trim conditions for a forward center-of-gravity position) this unstable pitching tendency did not occur because the control stalled first, producing a stable break in the pitching-moment curve. However, these static-stability data do not indicate what the dynamic behavior of the configuration would be at the stall, and it would be necessary to determine by other means whether undesirable control characteristics would result. In any case to obtain satisfactorily large lift coefficients for landing and for maneuvering while maintaining stick-fixed static longitudinal stability it would be necessary to increase appreciably the angle of attack at which the loss in lifting effectiveness of the wing developed. It is likely that by a change of airfoil section from the NACA 65-009 section of the test configuration a lift curve linear to considerably high angles of attack could be obtained. On either a canard or a conventional airplane with the test wing plan form the use of stall-control devices on the wing to delay and possibly reduce the unstable pitching tendency would be highly desirable.

3. The lift and pitching-moment data obtained at subsonic speeds by the wing-flow method were for the most part in good agreement with unpublished force-test data from the Langley free-flight tunnel.

Langley Aeronautical Laboratory  
National Advisory Committee for Aeronautics  
Langley Air Force Base, Va.

## APPENDIX I

## SYMBOLS

The following symbols and coefficients are used in this report:

L	lift, lb
N	normal force, lb
M'	pitching moment, ft-lb
W	weight, lb
L'	rolling moment, ft-lb
C	chord force, lb
D	drag, lb
M	model Mach number
M <sub>F</sub>	airplane Mach number
R	Reynolds number
c	wing chord, ft
$\bar{c}$	mean aerodynamic chord (mean geometric chord), ft
b	wing span, ft
$i_t$	control incidence or deflection, deg
$\alpha$	model angle of attack, deg
S	wing area, sq ft
S <sub>t</sub>	control-surface area, sq ft
$\rho$	density of air, slugs/cu ft
V	true airspeed, fps
q	dynamic pressure, lb/sq ft $\left(\frac{1}{2}\rho V^2\right)$

$C_N$	normal-force coefficient $\left(\frac{N}{qS}\right)$
$C_L$	lift coefficient $\left(\frac{L}{qS}\right)$
$C_m$	pitching-moment coefficient (about a point 40 percent chord ahead of the leading edge of the mean geometric chord) $\left(\frac{M}{qSc}\right)$
$C_l$	rolling-moment coefficient $\left(\frac{L'}{qSb}\right)$
$C_c$	chord-force coefficient $\left(\frac{C}{qS}\right)$
$C_D$	drag coefficient $\left(\frac{D}{qS}\right)$
$\frac{\partial C_m}{\partial C_L}$	rate of change of pitching moment measured about an axis 40 percent chord ahead of the mean aerodynamic chord (-40 percent $\bar{C}$ ) with lift coefficient
$C_{L\alpha}$	rate of change of lift coefficient with angle of attack, per deg
$C_{m\alpha}$	rate of change of pitching-moment coefficient with angle of attack, per deg
$C_{l\alpha}$	rate of change of rolling-moment coefficient with angle of attack, per deg
$C_{m_{it}}$	rate of change of pitching-moment coefficient with control incidence, per deg
$\Delta\bar{x}$	center-of-gravity shift, ft
$n$	load factor
$g$	acceleration of gravity
$l_t$	distance from model pivot point at -40 percent $\bar{C}$ to the aerodynamic center of the control surface
$H$	pressure altitude, ft

## APPENDIX II

## EXPRESSION FOR CALCULATION OF TRIM CURVES

The expression for the calculation of stabilizer settings for trim from the data of figures 7, 8, and 10 was derived from a summation of moment as follows:

$$\Sigma M' = 0$$

$$M_A - W_n \bar{\Delta x} + M_{it} = 0$$

where  $M_A$  is the untrimmed pitching moment about -40 percent  $\bar{c}$  as given in figures 7 and 8,  $W_n \bar{\Delta x}$  is the increment of moment due to shift of the center-of-gravity position, (this term must be included to obtain trim curves at other than the test center-of-gravity position) and  $M_{it}$  is the trimming moment supplied by proper deflection of the control surface. In coefficient form the expression becomes

$$C_{m_A} - C_{L_T} \frac{\bar{\Delta x}}{c} + C_{m_{it}} i_t = 0$$

in which  $C_{L_T}$  is the total or trimmed lift coefficient. To eliminate  $C_{L_T}$  from the expression

$$C_{L_T} = C_{L_A} + C_{L_{it}} i_t$$

or for more convenient use of the data presented

$$C_{L_T} = C_{L_A} + C_{m_{it}} i_t \frac{c}{l_t} \quad (1)$$

Then

$$C_{m_A} - \left( C_{L_A} + C_{m_{it}} i_t \frac{c}{l_t} \right) \frac{\bar{\Delta x}}{c} + C_{m_{it}} i_t = 0$$

Solving this expression

$$i_t = \frac{C_{L_A} \frac{\Delta \bar{x}}{c} - C_{m_A}}{C_{m_{i_t}} \left( 1 - \frac{\Delta \bar{x}}{l_t} \right)} \quad (2)$$

In order to calculate trim curves from the data presented, the initial stabilizer setting of  $1.8^\circ$  must be considered by modifying expressions (1) and (2) as follows:

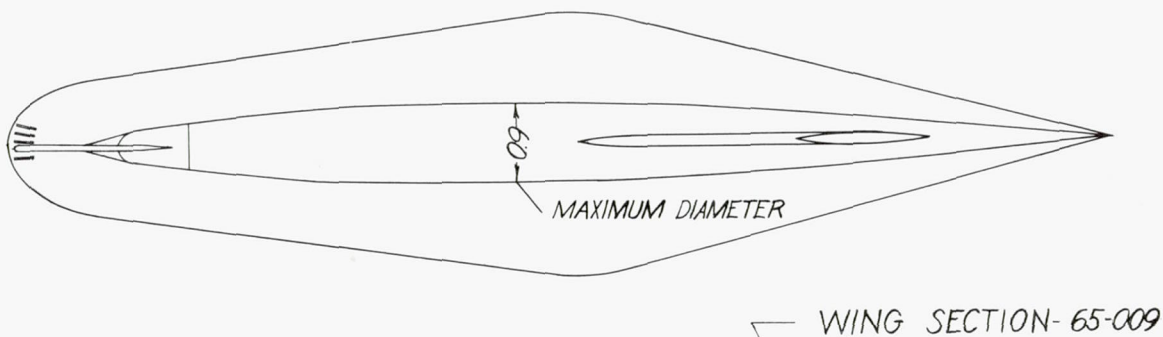
$$C_{L_T} = C_{L_A} + C_{m_{i_t}} (i_t - 1.8) \frac{c}{l_t}$$

$$i_t = 1.8 + \frac{C_{L_A} \frac{\Delta \bar{x}}{c} - C_{m_A}}{C_{m_{i_t}} \left( 1 - \frac{\Delta \bar{x}}{l_t} \right)}$$

It should be noted that a method of successive approximations is required to determine  $i_t$  at a specified trimmed lift coefficient.

## REFERENCES

1. Mathews, Charles W.: Study of the Canard Configuration with Particular Reference to Transonic Flight Characteristics and Low-Speed Characteristics at High Lift. NACA RM L8G14, 1949.
2. Kraft, Christopher C., Jr., and Mathews, Charles W.: Determination by the Free-Fall Method of the Drag and Longitudinal Stability and Control Characteristics of a Canard Model at Transonic Speeds. NACA RM L50D04, 1950.
3. Riebe, John M., and Fikes, Joseph E.: Preliminary Aerodynamic Investigation of the Effect of Camber on a 60° Delta Wing with Round and Beveled Leading Edges. NACA RM L9F10, 1949.
4. Graham, Robert R., and Connor, D. William: Investigation of High-Lift and Stall-Control Devices on an NACA 64-Series 42° Sweptback Wing with and without Fuselage. NACA RM L7G09, 1947.
5. Neely, Robert H., and Koven, William: Low-Speed Characteristics in Pitch of a 42° Sweptback Wing with Aspect Ratio 3.9 and Circular-Arc Airfoil Sections. NACA RM L7E23, 1947.



ASPECT RATIO = 4.1  
 WING AREA ,  $S = .0334 \text{ ft}^2$   
 TAIL AREA ,  $S_t = .0056 \text{ ft}^2$

ALL DIMENSIONS IN INCHES

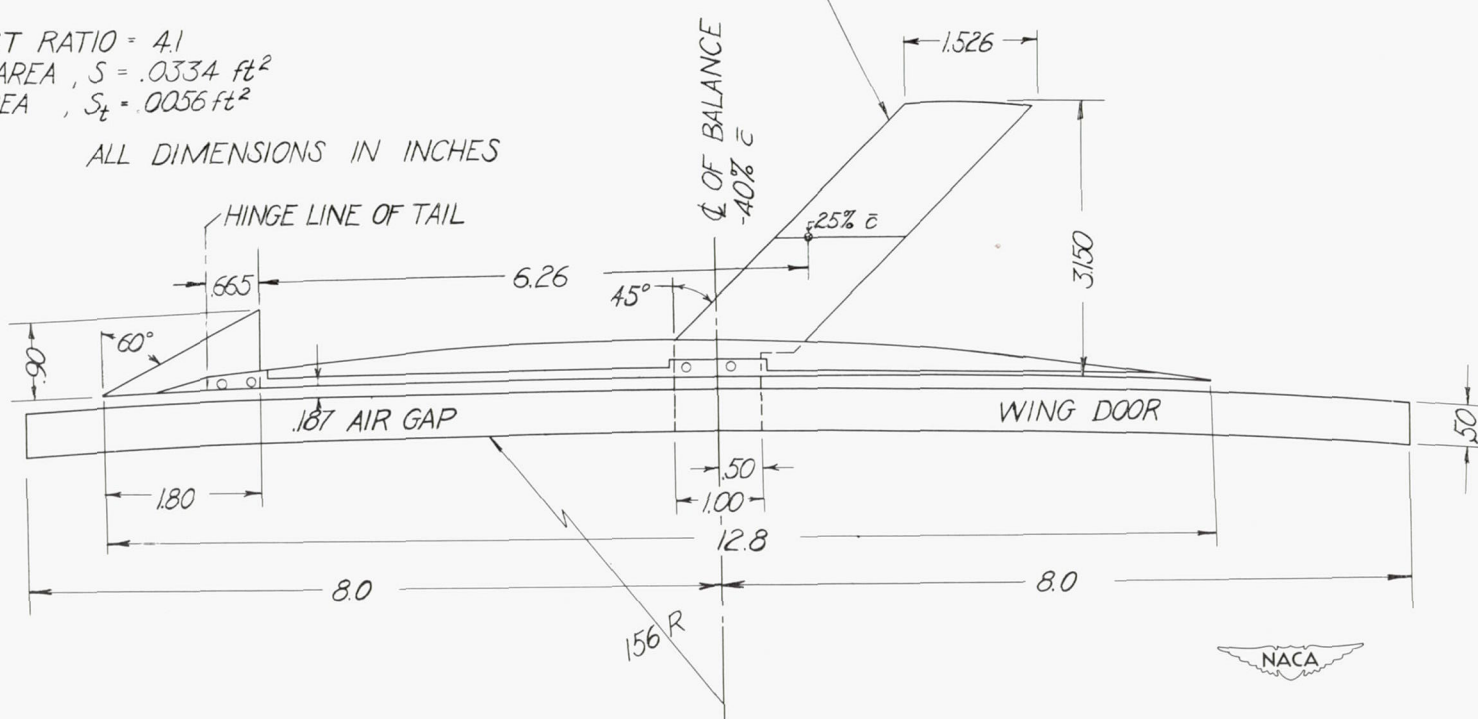


Figure 1.-- Sketch of model of canard airplane configuration.

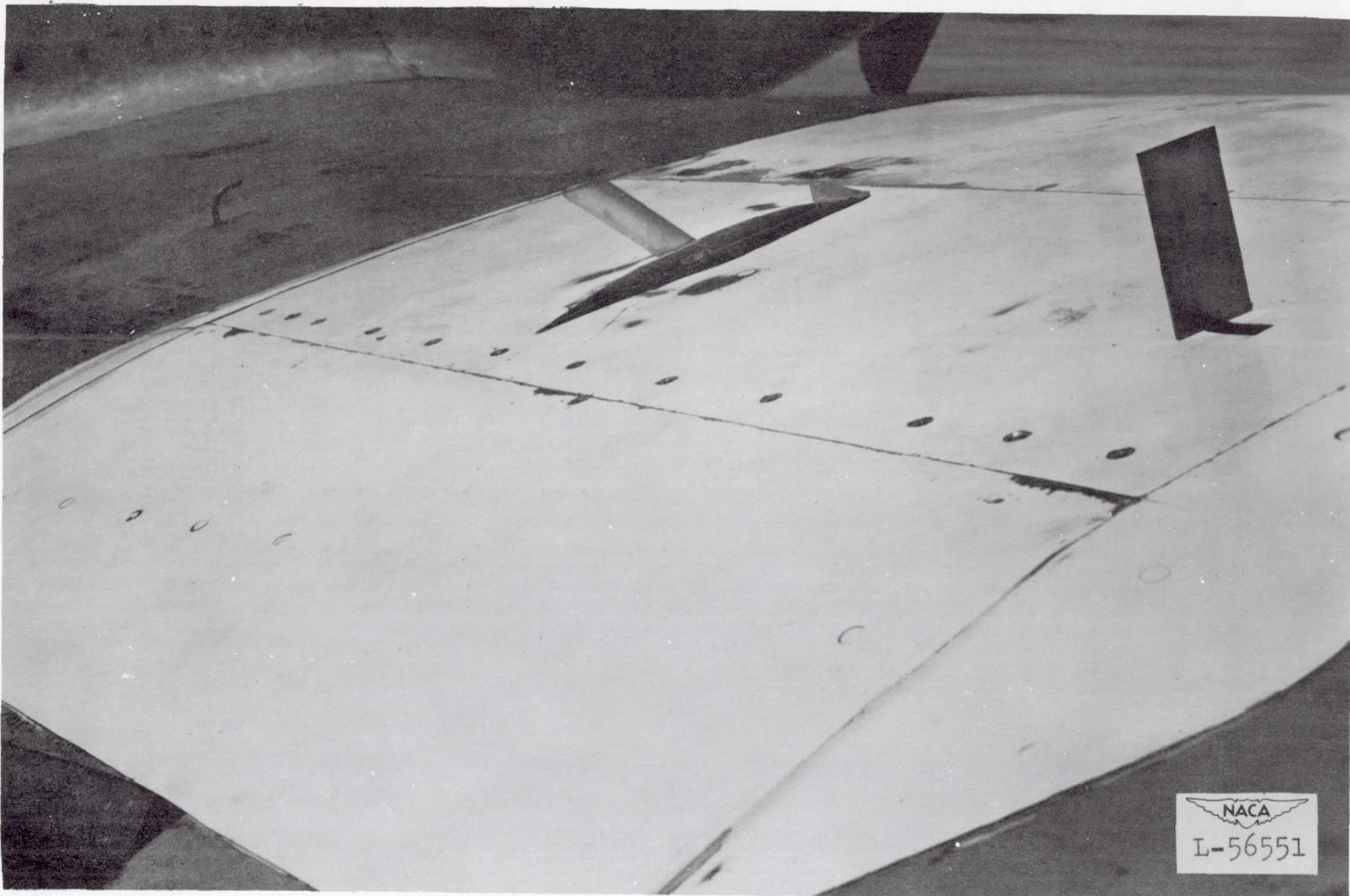
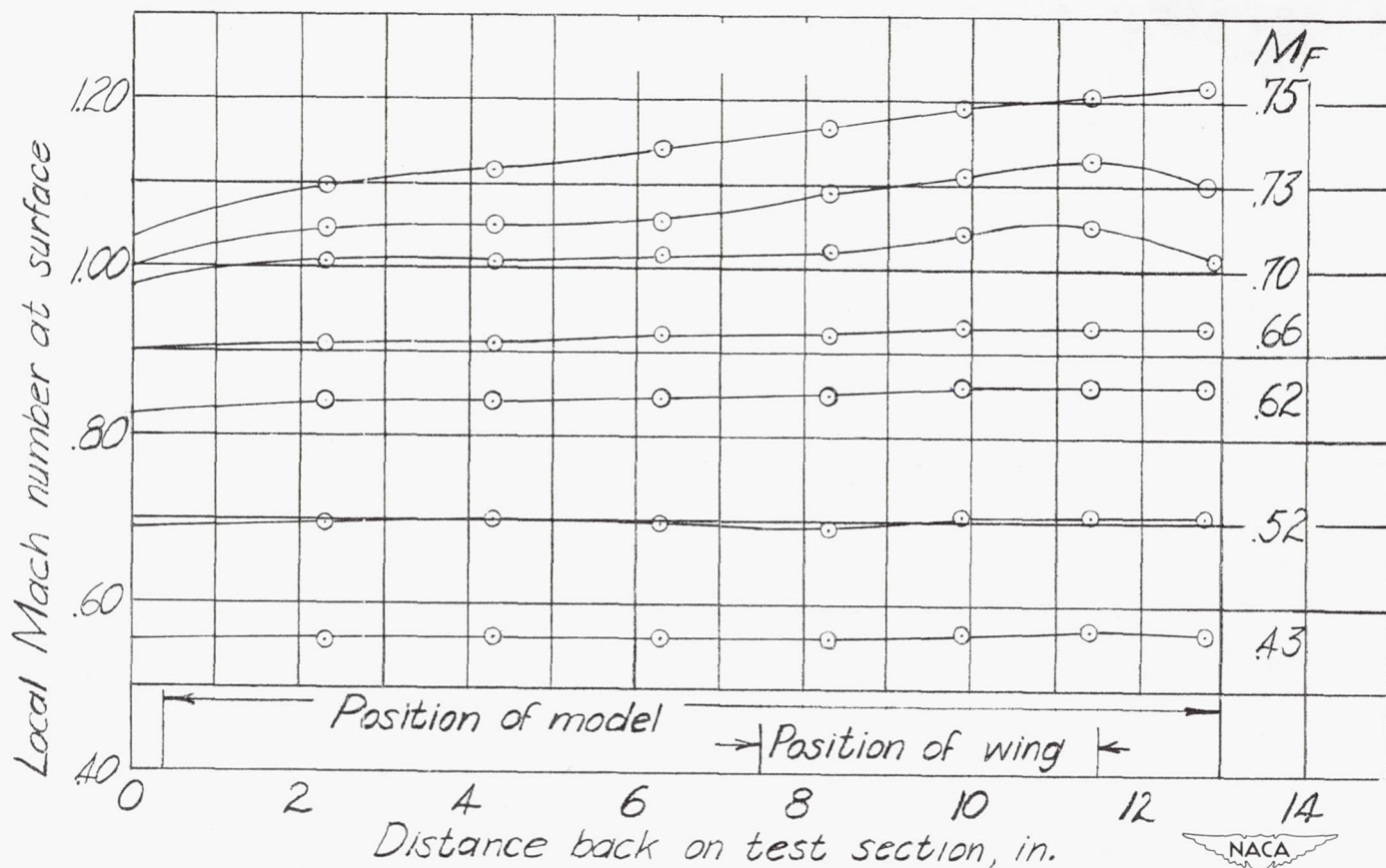


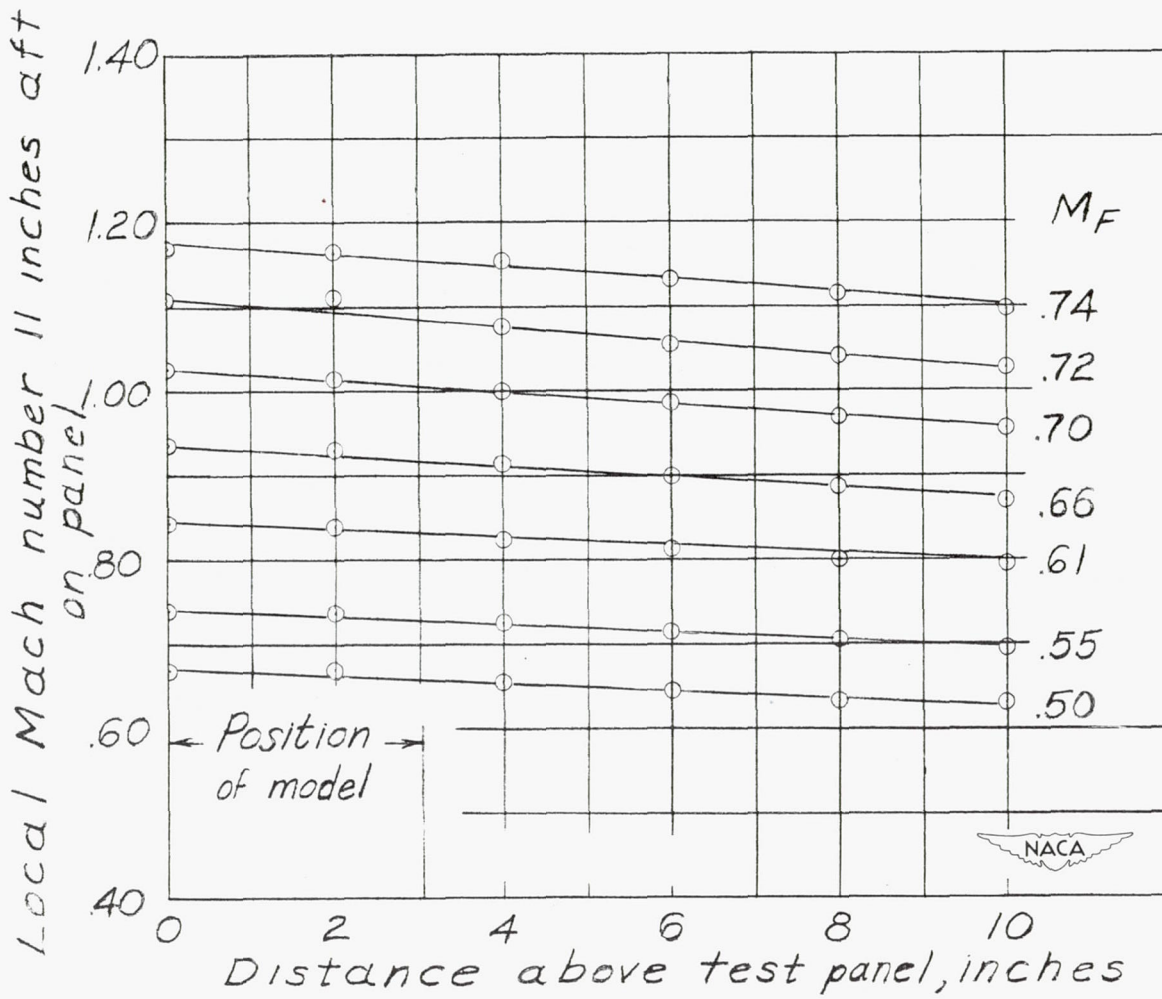
Figure 2.— Photograph of canard model in place on test panel.





(a) Horizontal.

Figure 3.— Velocity gradients over F-51D wing-flow test panel.



(b) Vertical.

Figure 3.- Concluded.

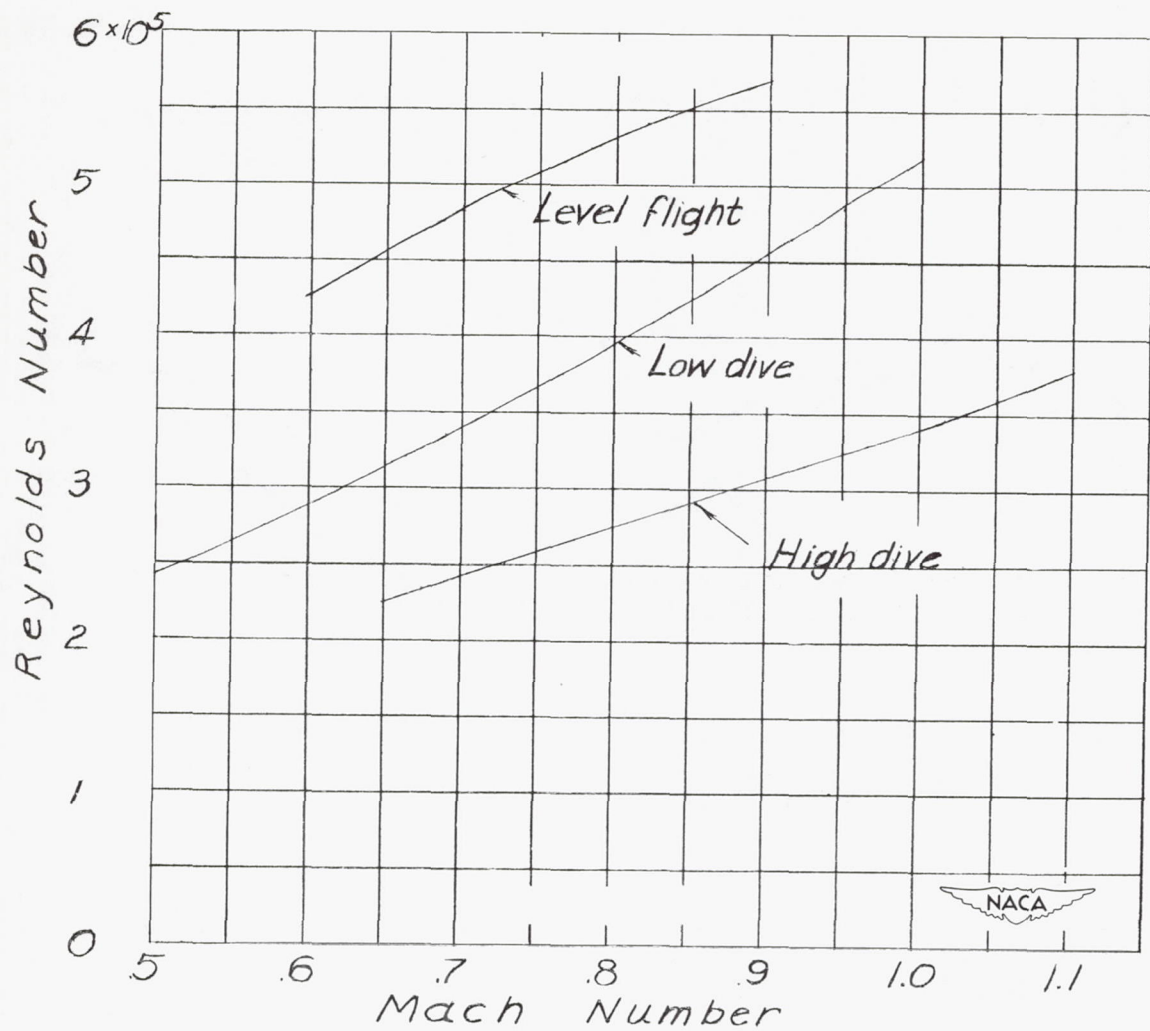


Figure 4.— Variation of Reynolds number with Mach number during wing-flow tests of canard airplane configuration.

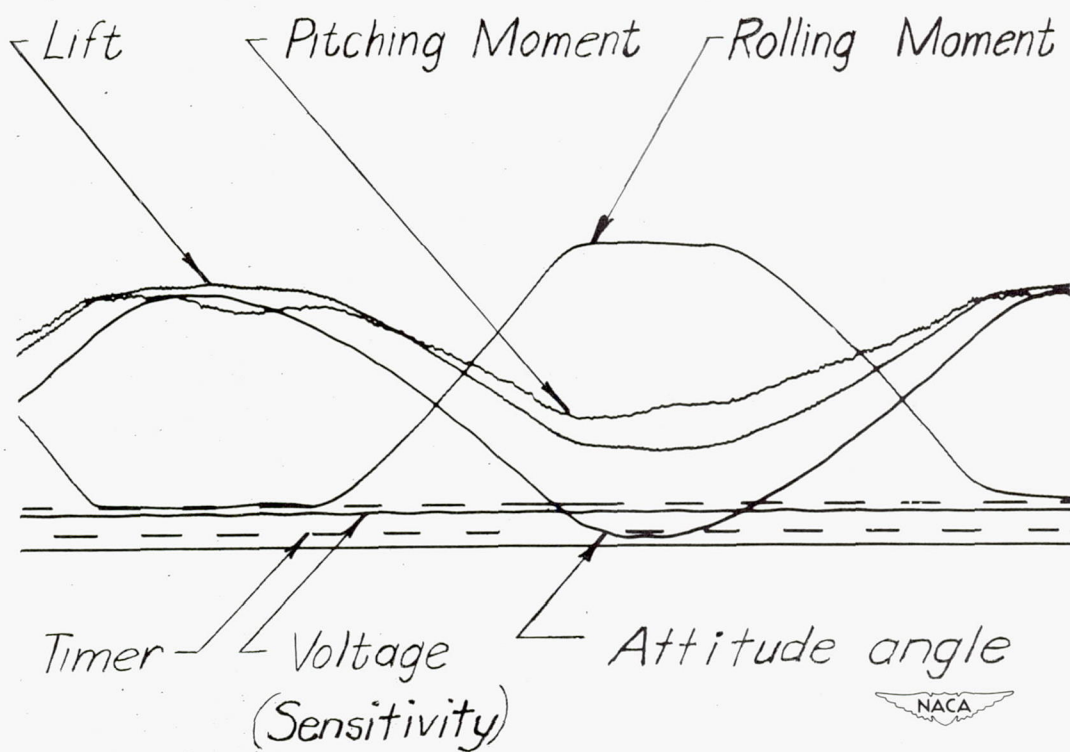


Figure 5.- Sample galvanometer record from the strain-gage balance used during a portion of the wing-flow tests of the canard airplane configuration.

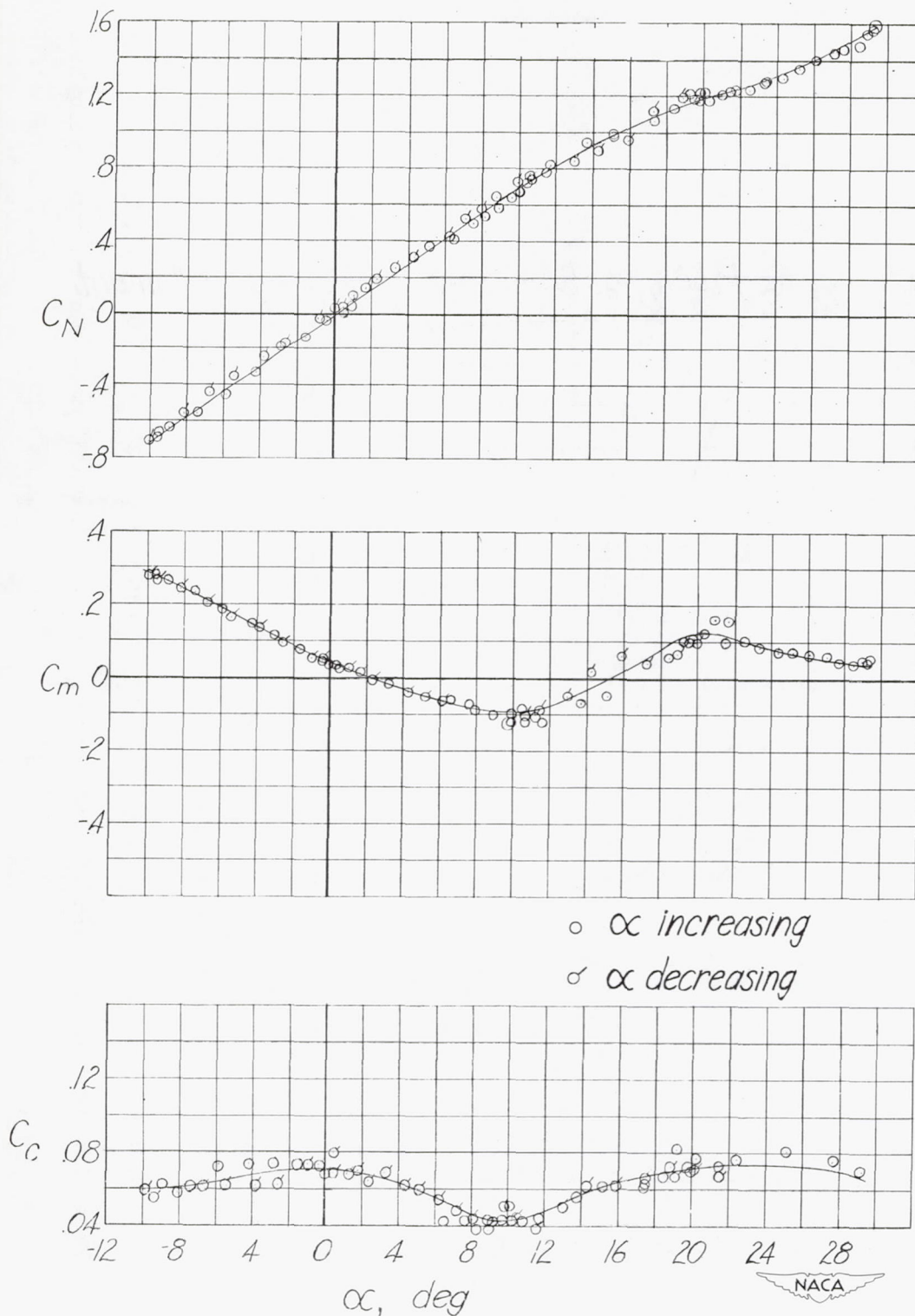
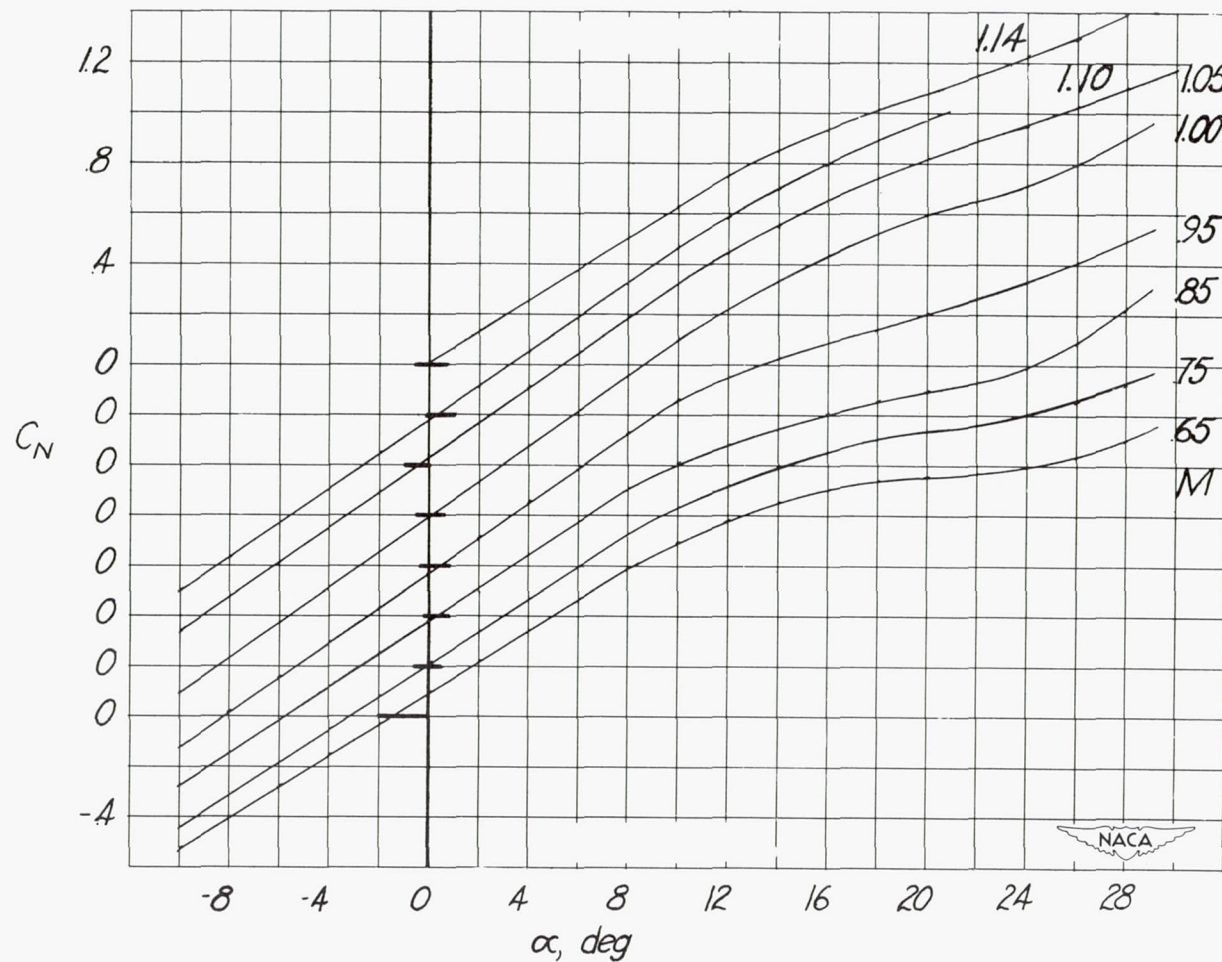
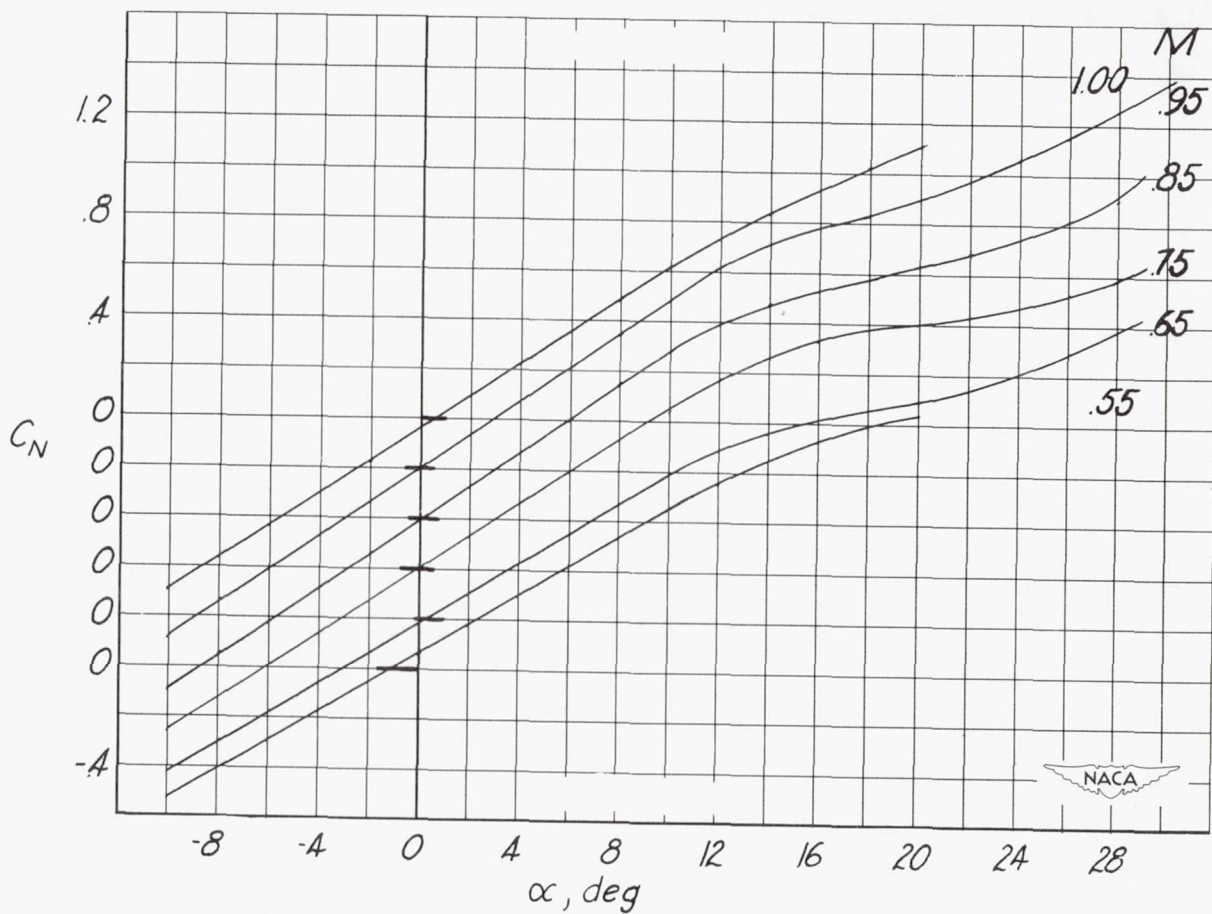


Figure 6.— Typical wing-flow data for canard airplane configuration with the control surface deflected  $1.8^\circ$  at  $M = 1.0$ .



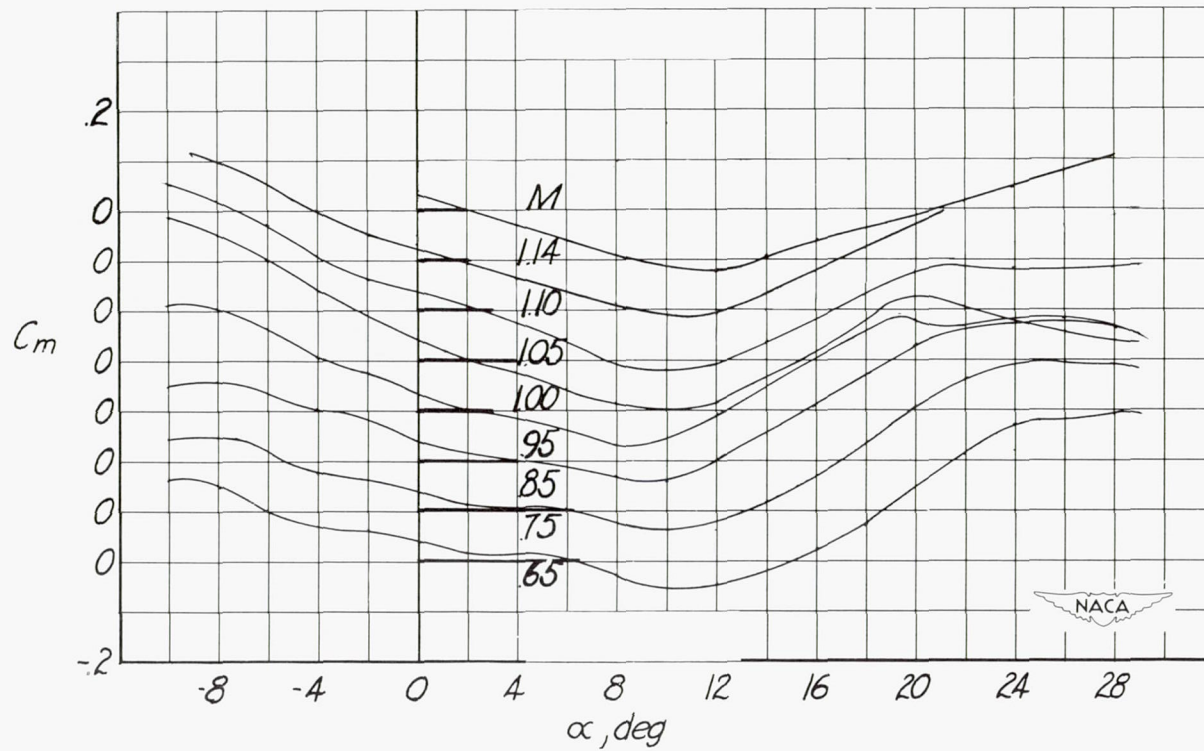
(a) Normal-force coefficient, Reynolds number range  $2.2 \times 10^5$  to  $3.8 \times 10^5$ .

Figure 7.— Wing-flow data from canard airplane configuration at several Mach numbers for a stabilizer setting of  $1.8^\circ$ .



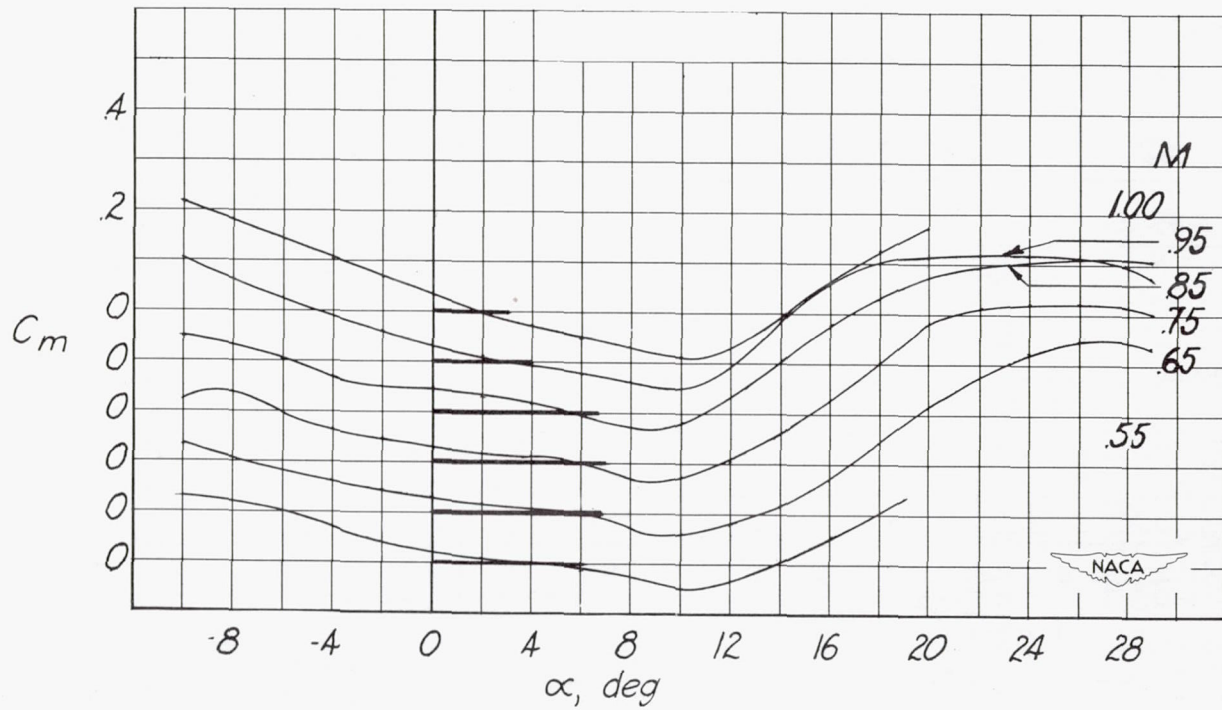
(b) Normal-force coefficient, Reynolds number range  $2.4 \times 10^5$  to  $5.2 \times 10^5$ .

Figure 7.—Continued.



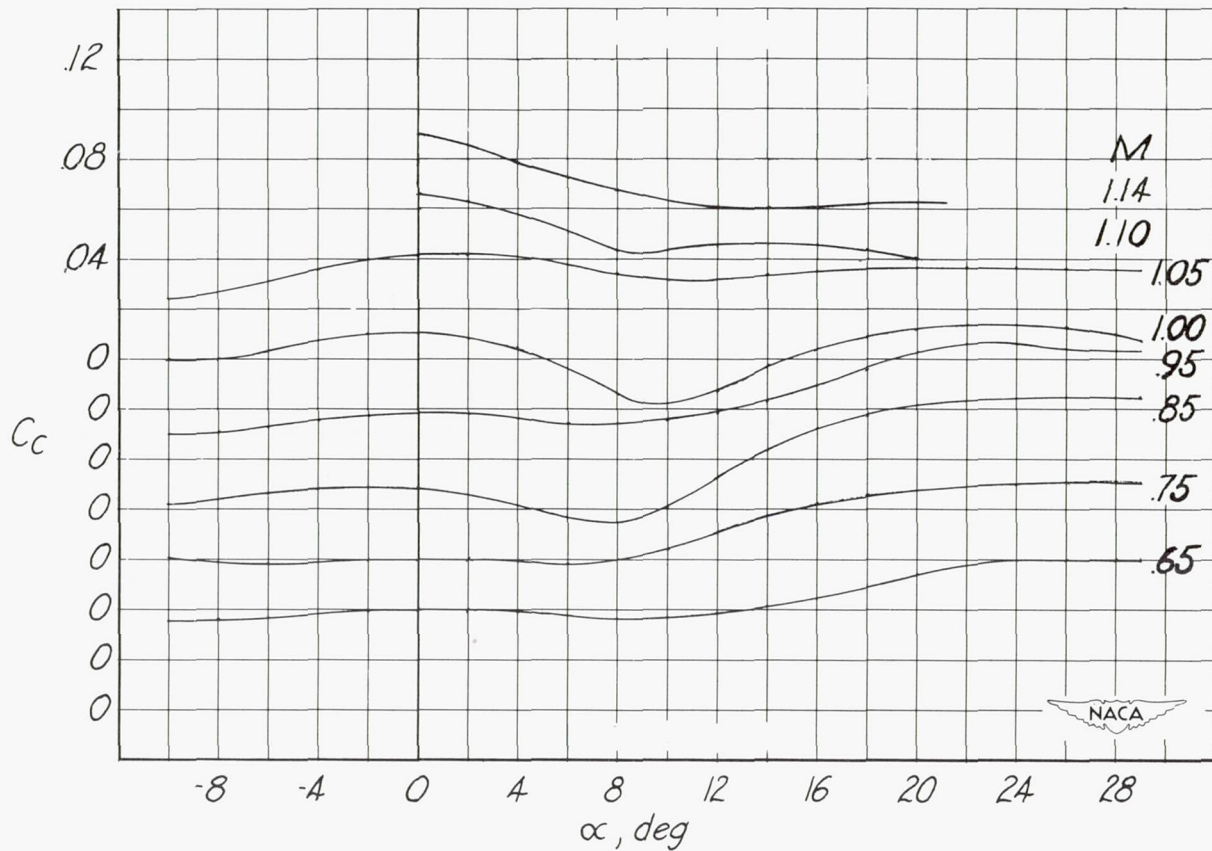
(c) Pitching-moment coefficient, Reynolds number range  $2.2 \times 10^5$  to  $3.8 \times 10^5$ .

Figure 7.— Continued.



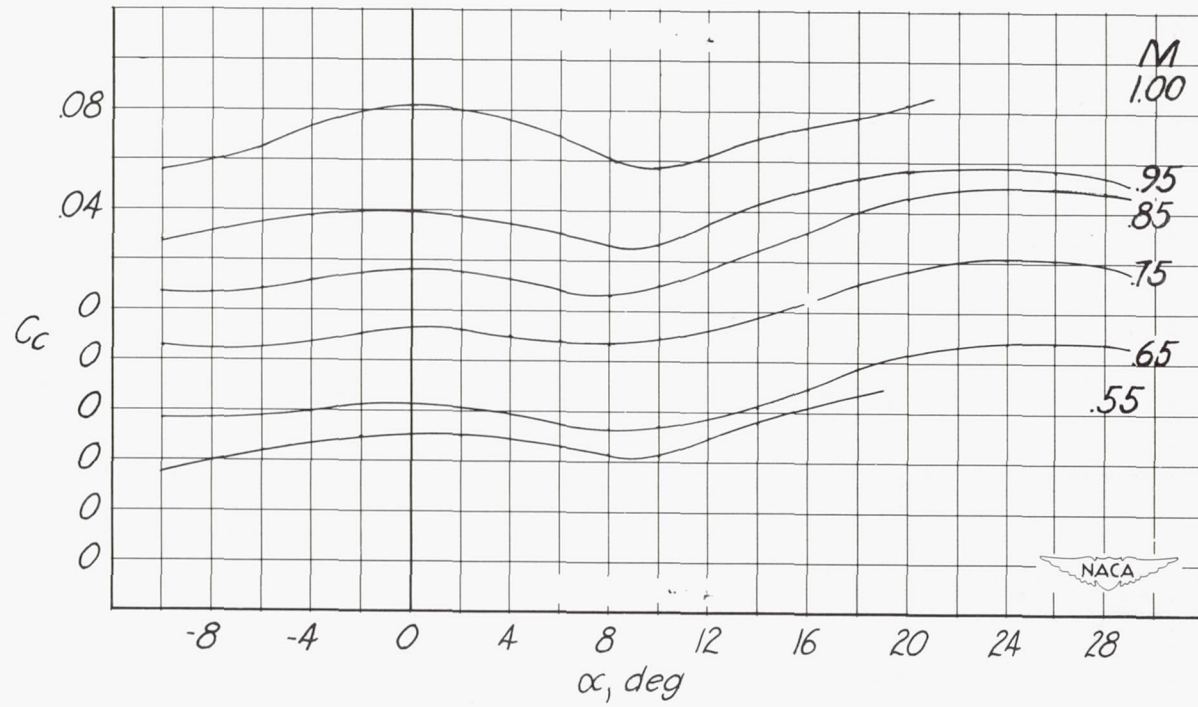
(d) Pitching-moment coefficient, Reynolds number range  $2.4 \times 10^5$  to  $5.2 \times 10^5$ .

Figure 7.—Continued.



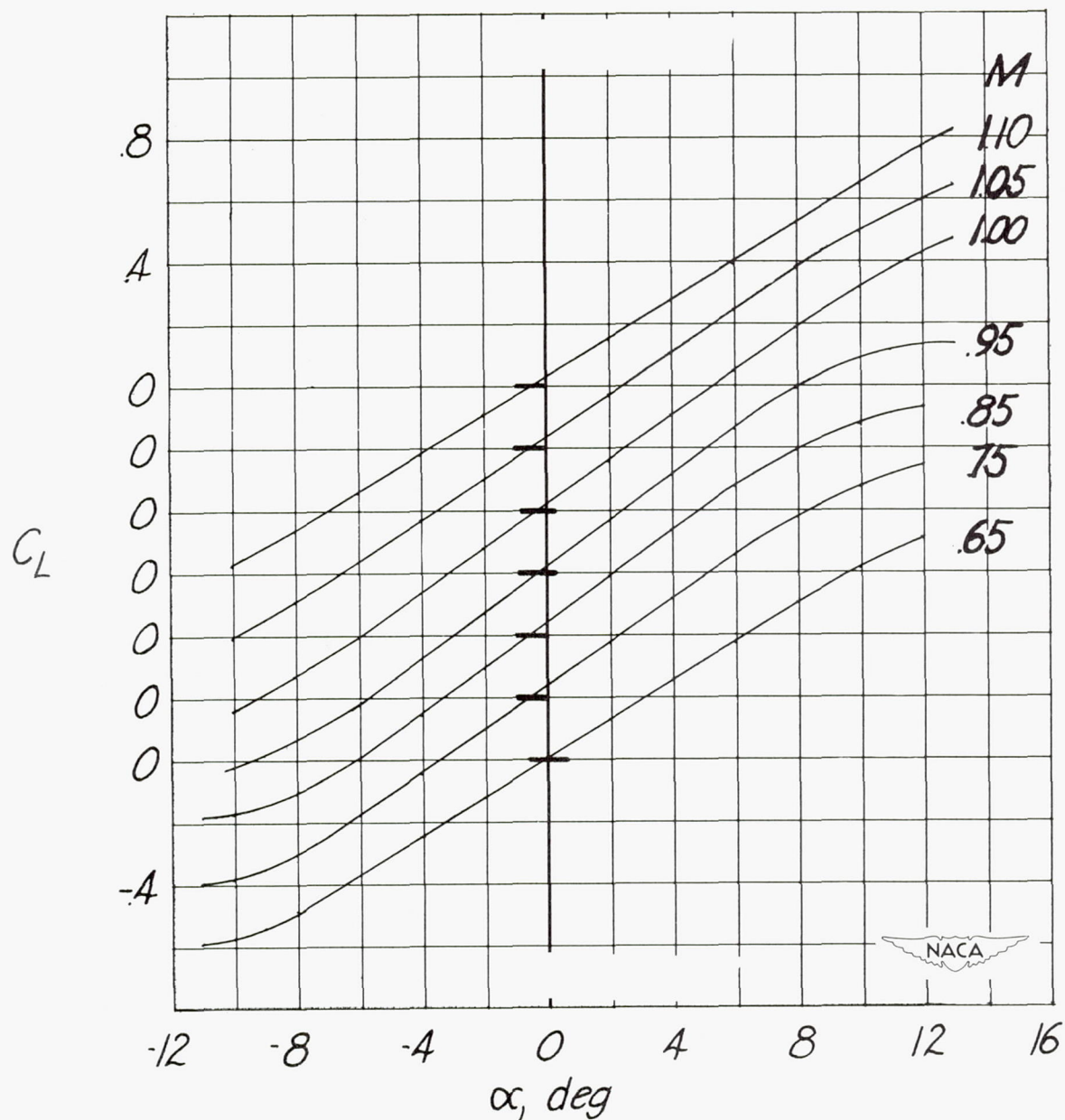
(e) Chord-force coefficient, Reynolds number range  $2.2 \times 10^5$  to  $3.8 \times 10^5$ .

Figure 7.- Continued.



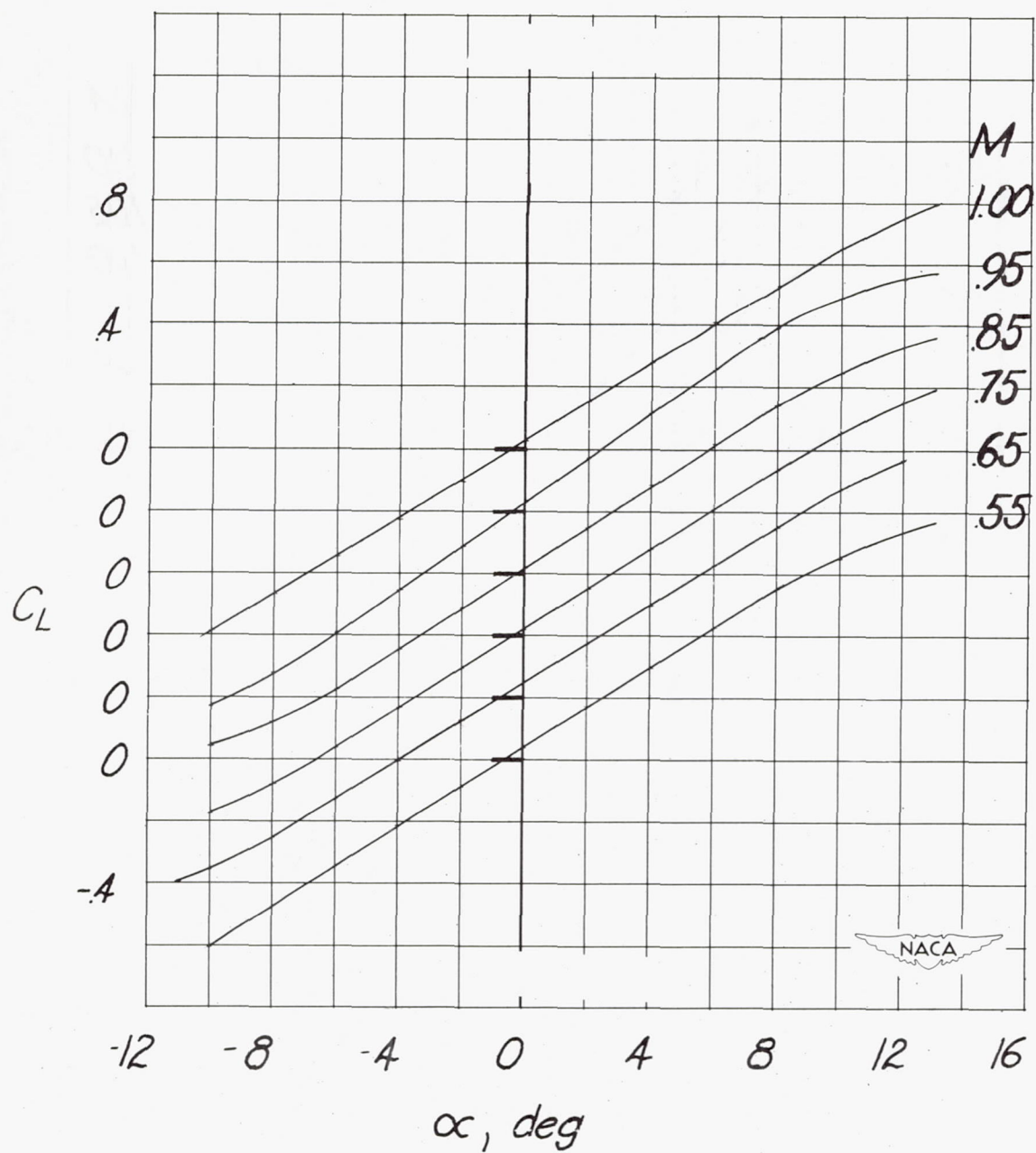
(f) Chord-force coefficient, Reynolds number range  $2.4 \times 10^5$  to  $5.2 \times 10^5$ .

Figure 7.— Concluded.



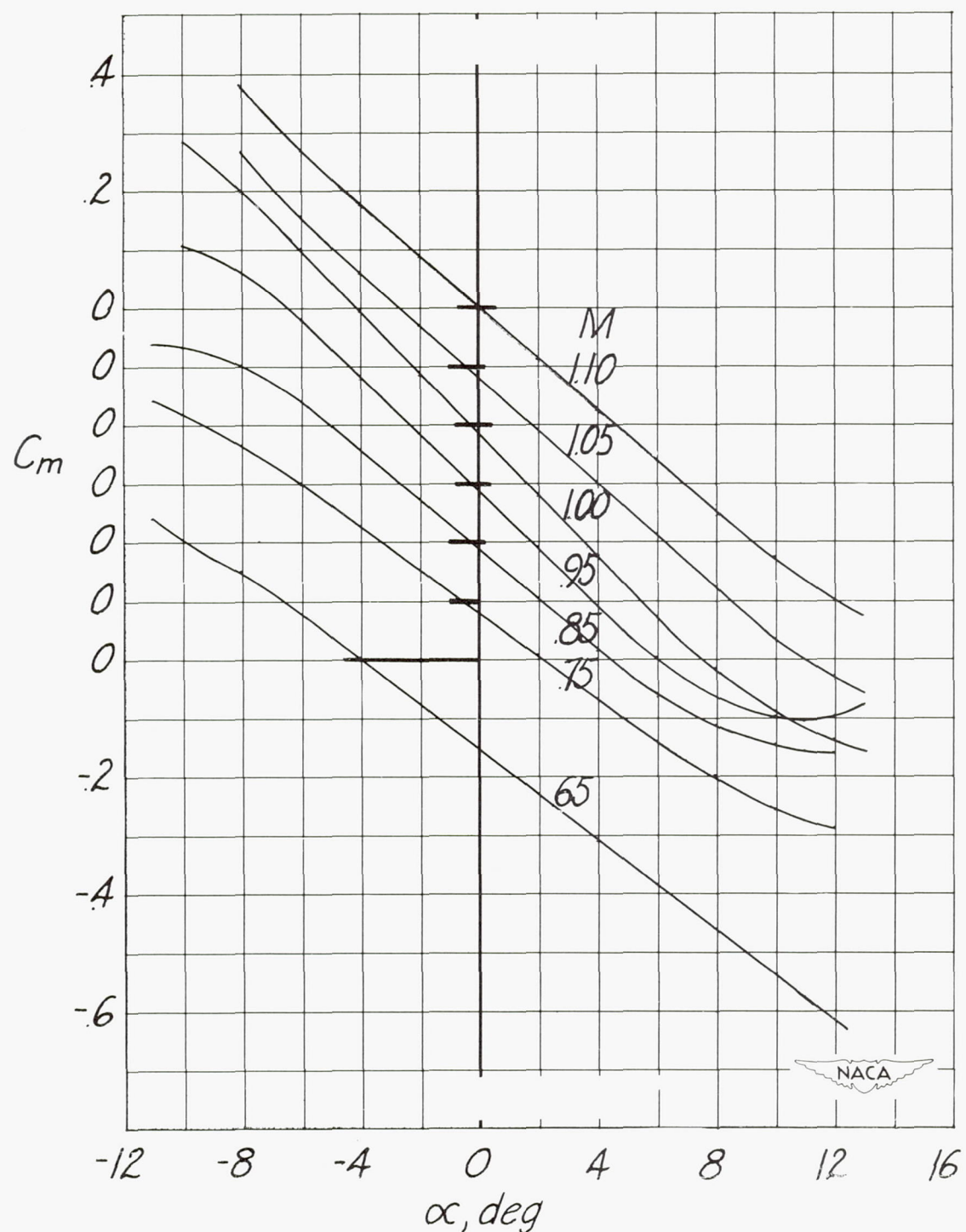
(a) Lift coefficient, Reynolds number range  $2.2 \times 10^5$  to  $3.8 \times 10^5$ .

Figure 8.— Wing-flow data from canard airplane configuration at several Mach numbers with stabilizer removed.



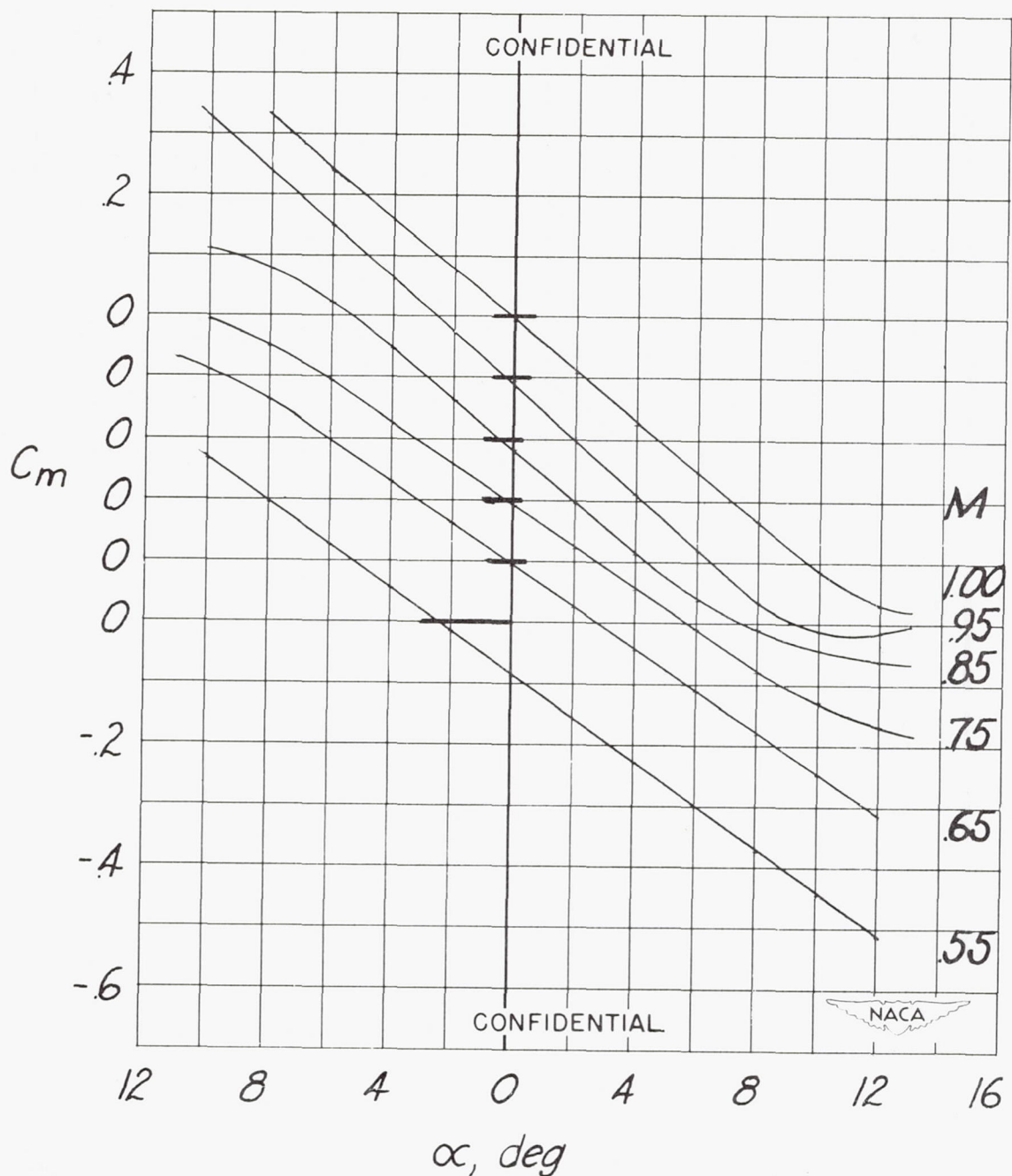
(b) Lift coefficient, Reynolds number range  $2.4 \times 10^5$  to  $5.2 \times 10^5$ .

Figure 8.- Continued.



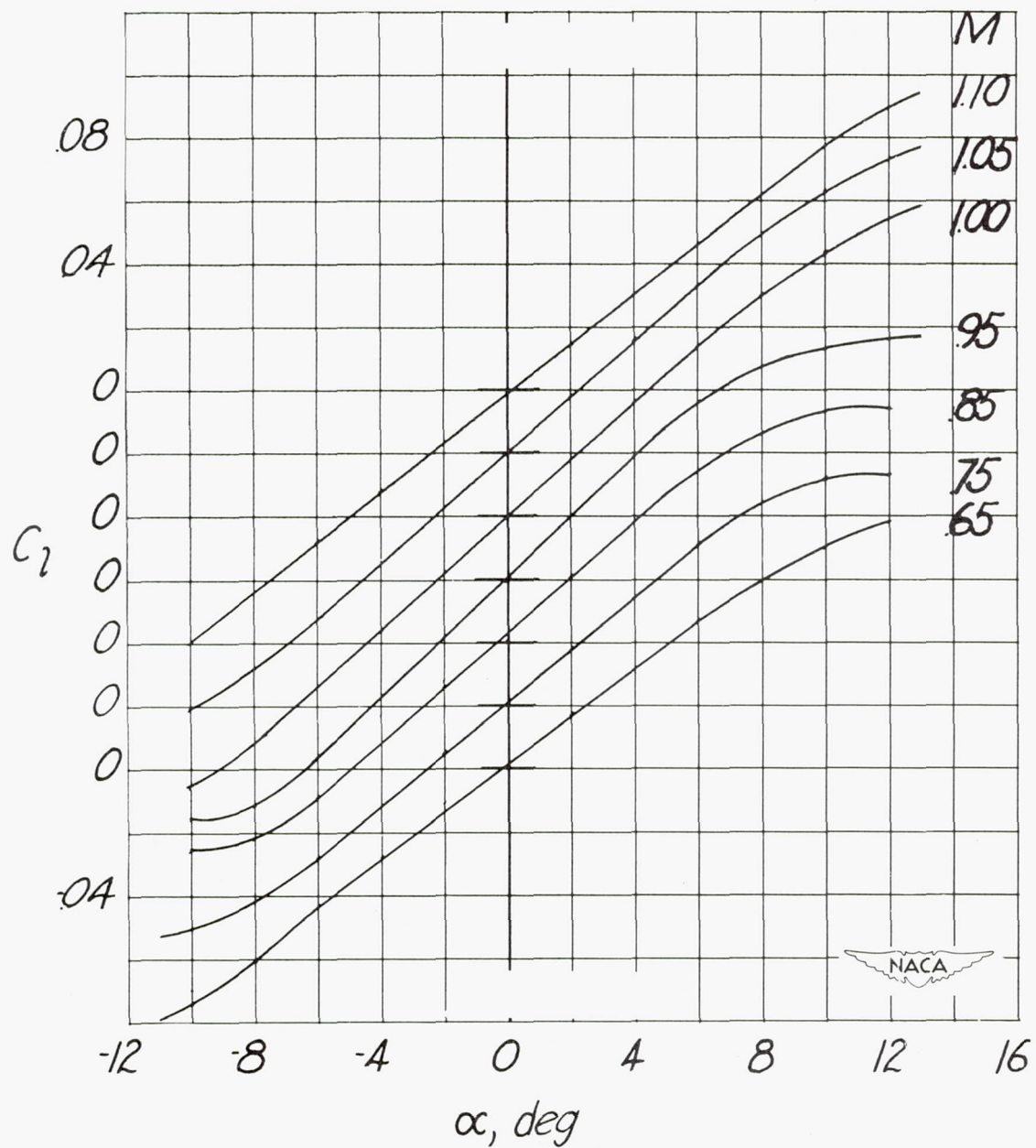
(c) Pitching-moment coefficient, Reynolds number range  $2.2 \times 10^5$  to  $3.8 \times 10^5$ .

Figure 8.— Continued.



(d) Pitching-moment coefficient, Reynolds number range  $2.4 \times 10^5$  to  $5.2 \times 10^5$ .

Figure 8.- Continued.



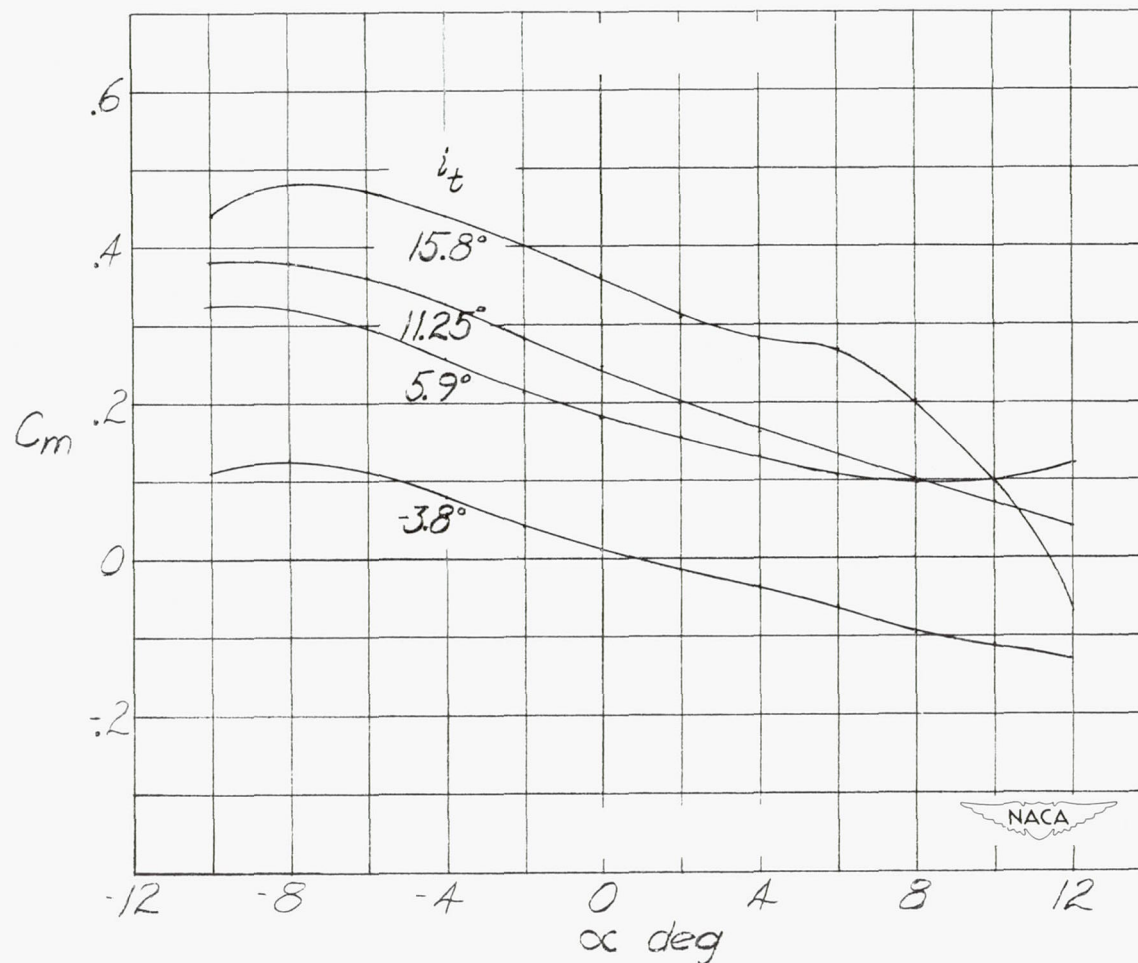
(e) Rolling-moment coefficient of half-span model, Reynolds number range  $2.2 \times 10^5$  to  $3.8 \times 10^5$ .

Figure 8.—Continued.



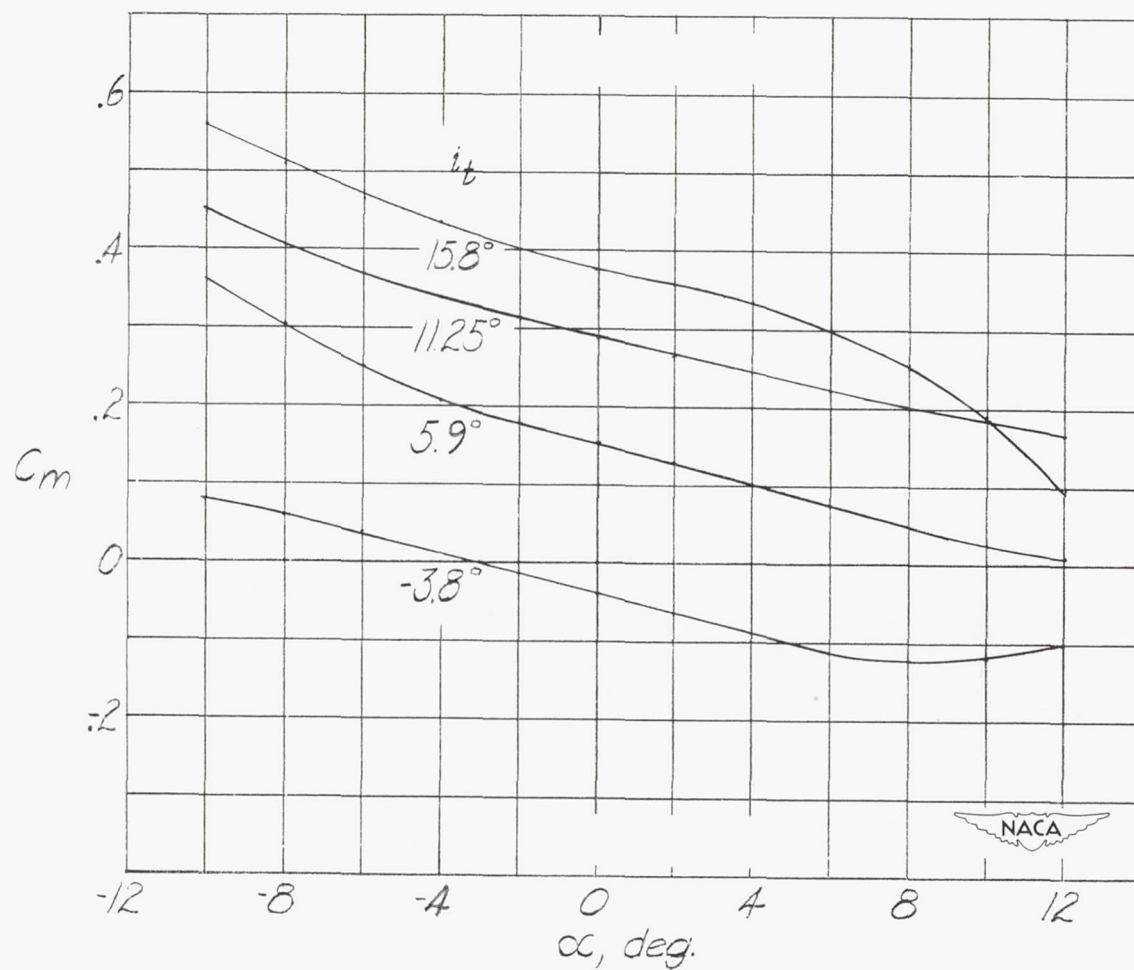
(f) Rolling-moment coefficient of semispan model, Reynolds number range  $2.4 \times 10^5$  to  $5.2 \times 10^5$ .

Figure 8.— Concluded.



(a) Reynolds number 2.2 to  $3.8 \times 10^5$ .

Figure 9.— Variation of pitching-moment coefficient with angle of attack at  $M = 0.9$  for several control deflections, canard airplane configuration.



(b) Reynolds number 2.4 to  $5.2 \times 10^5$ .

Figure 9.— Concluded.

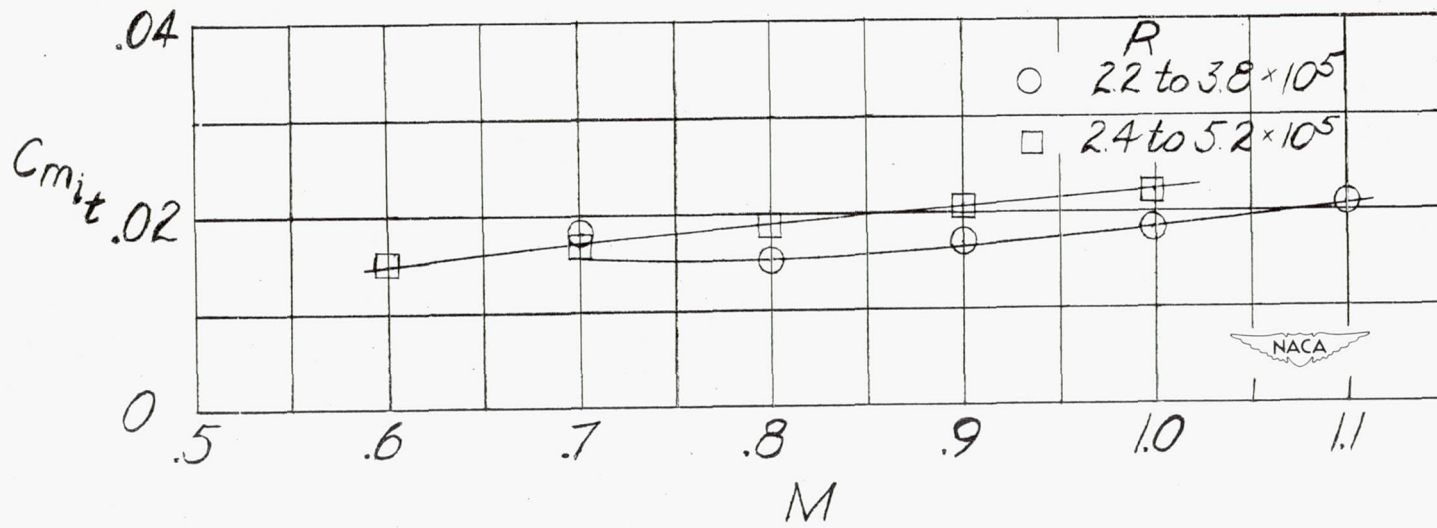


Figure 10.— Variation of stabilizer effectiveness with Mach number for canard airplane configuration.  
 $(\alpha + i_t < 25^\circ)$ .

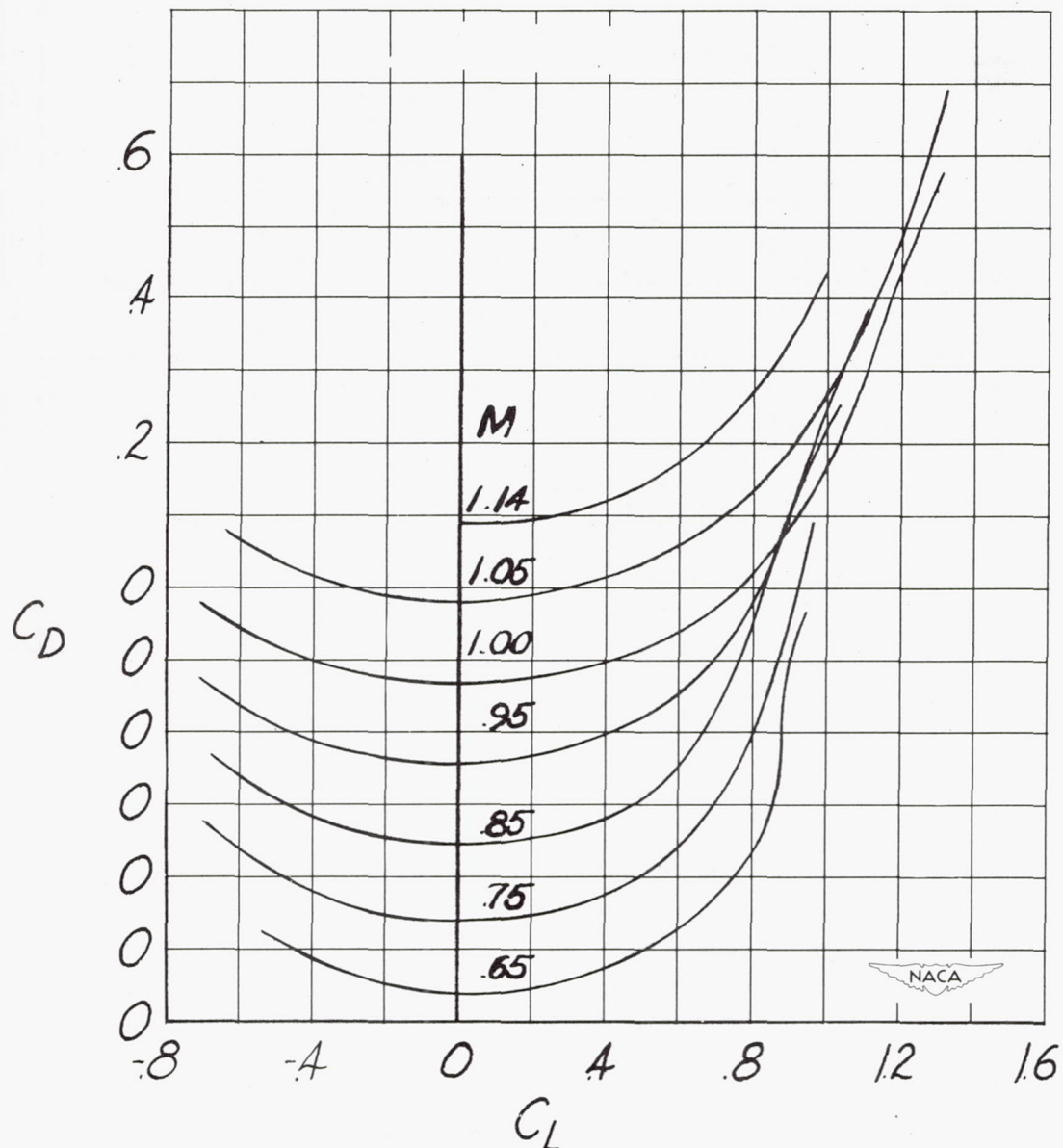


Figure 11.— Drag polars for canard airplane configuration at several Mach numbers for stabilizer setting of  $1.8^\circ$ .

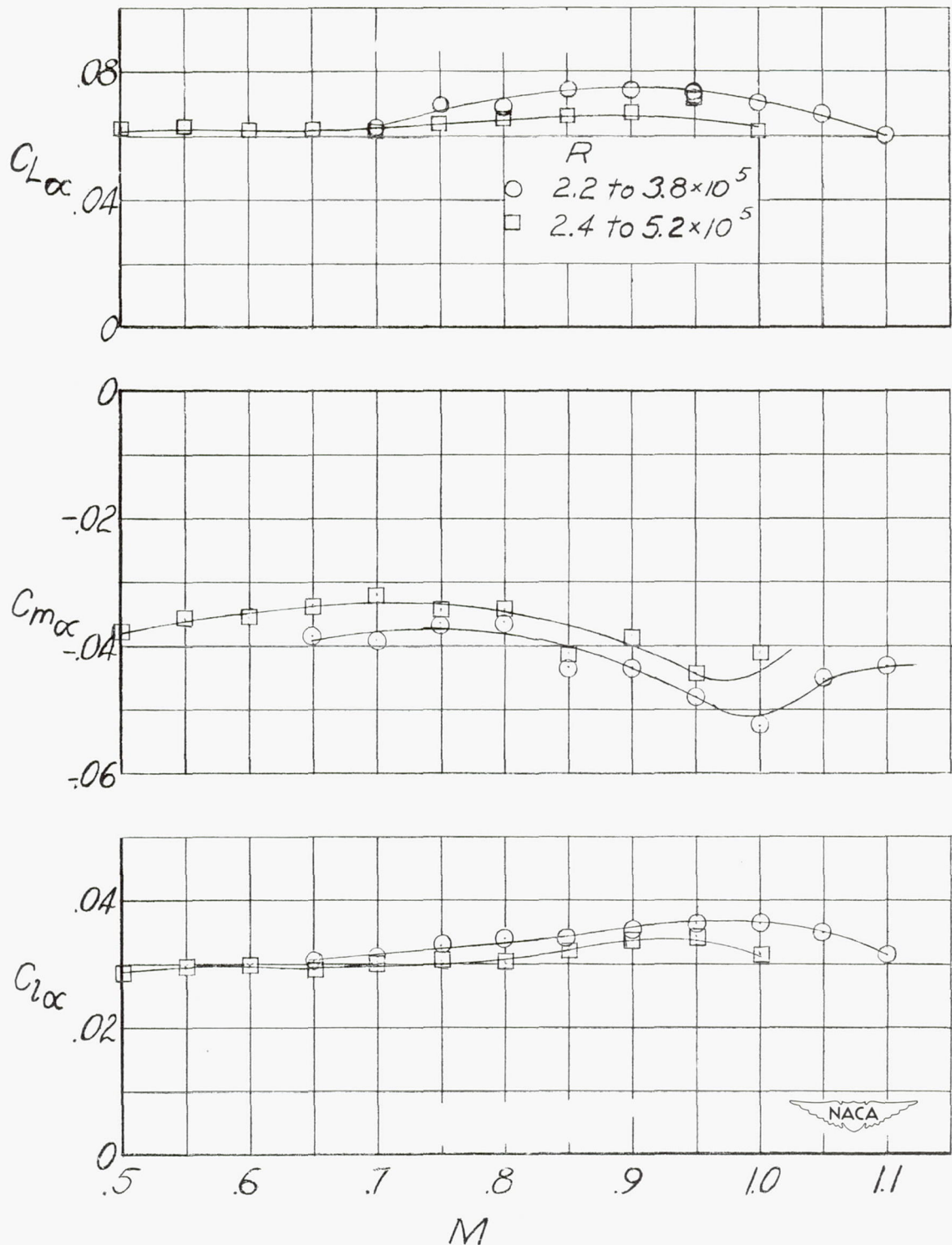
(a)  $C_{L\alpha}$ ,  $C_{m\alpha}$ , and  $C_{l\alpha}$  with stabilizer removed.

Figure 12.- Variation of longitudinal stability parameters with Mach number at a control-surface deflection of  $1.8^\circ$ .

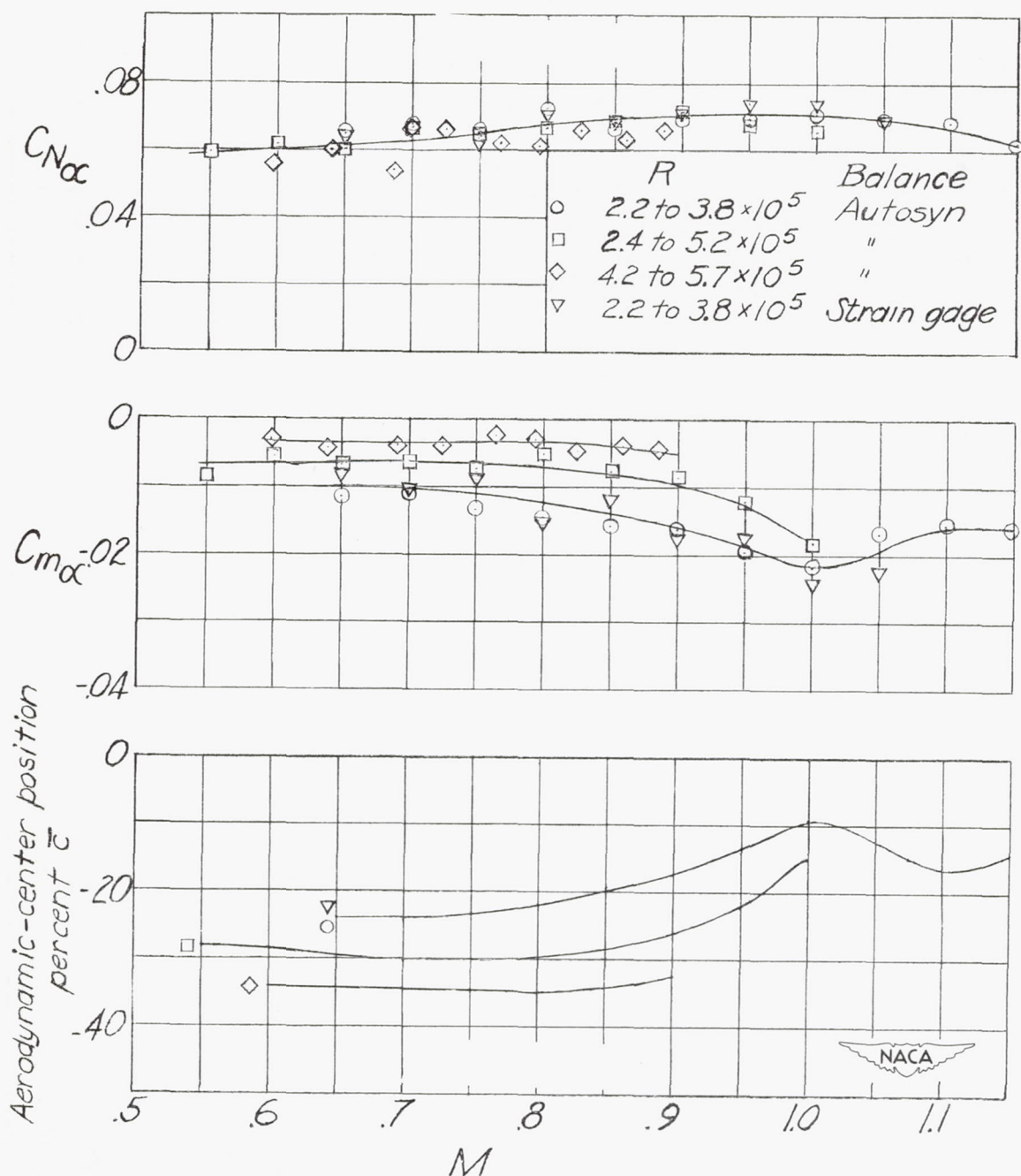
(b)  $C_{N\alpha}$ ,  $C_{m\alpha}$ , and  $\partial C_m / \partial C_N$  with stabilizer on.

Figure 12.- Concluded.

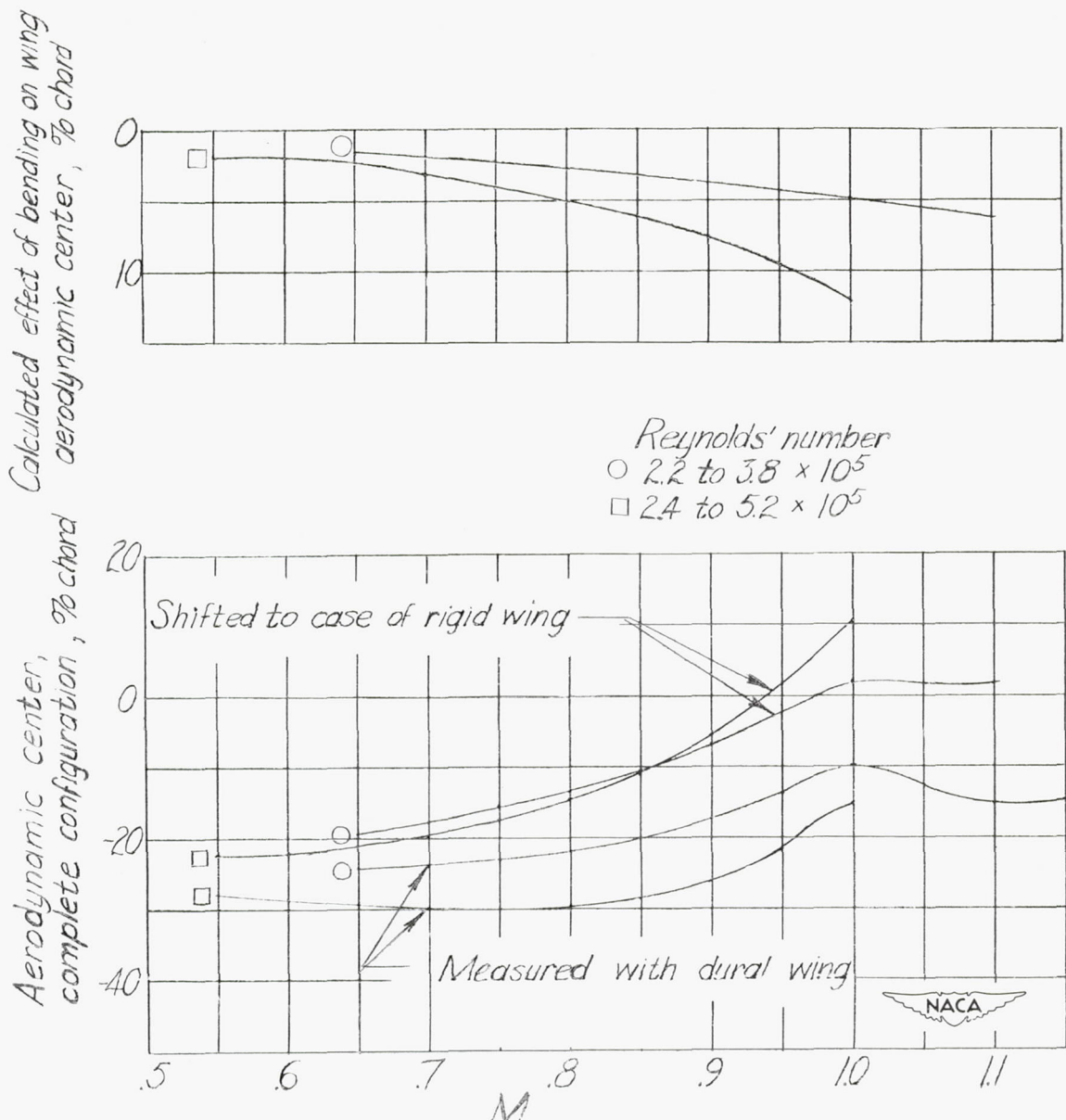


Figure 13.— Calculated effect of wing bending on aerodynamic-center position of canard airplane configuration.

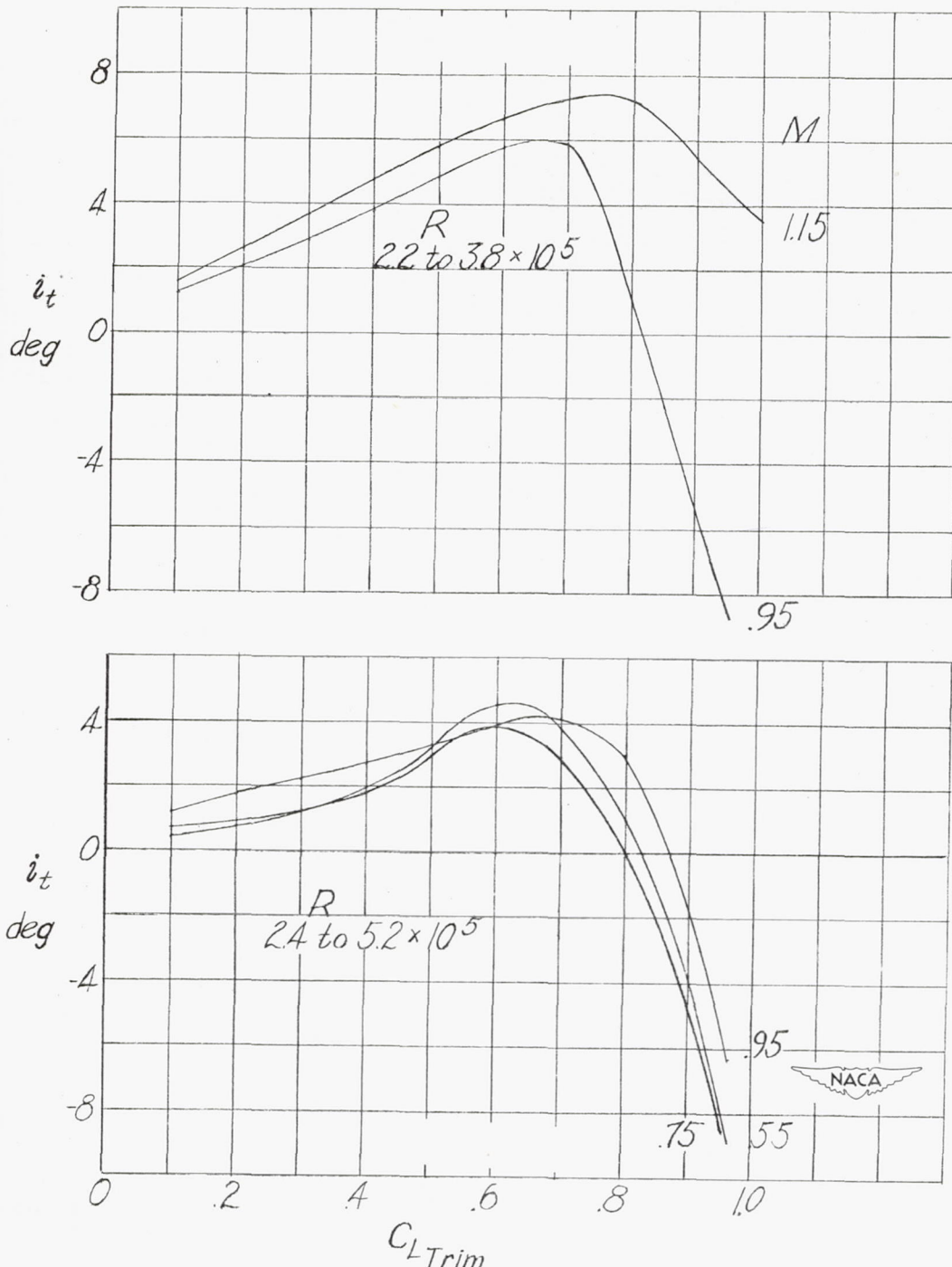
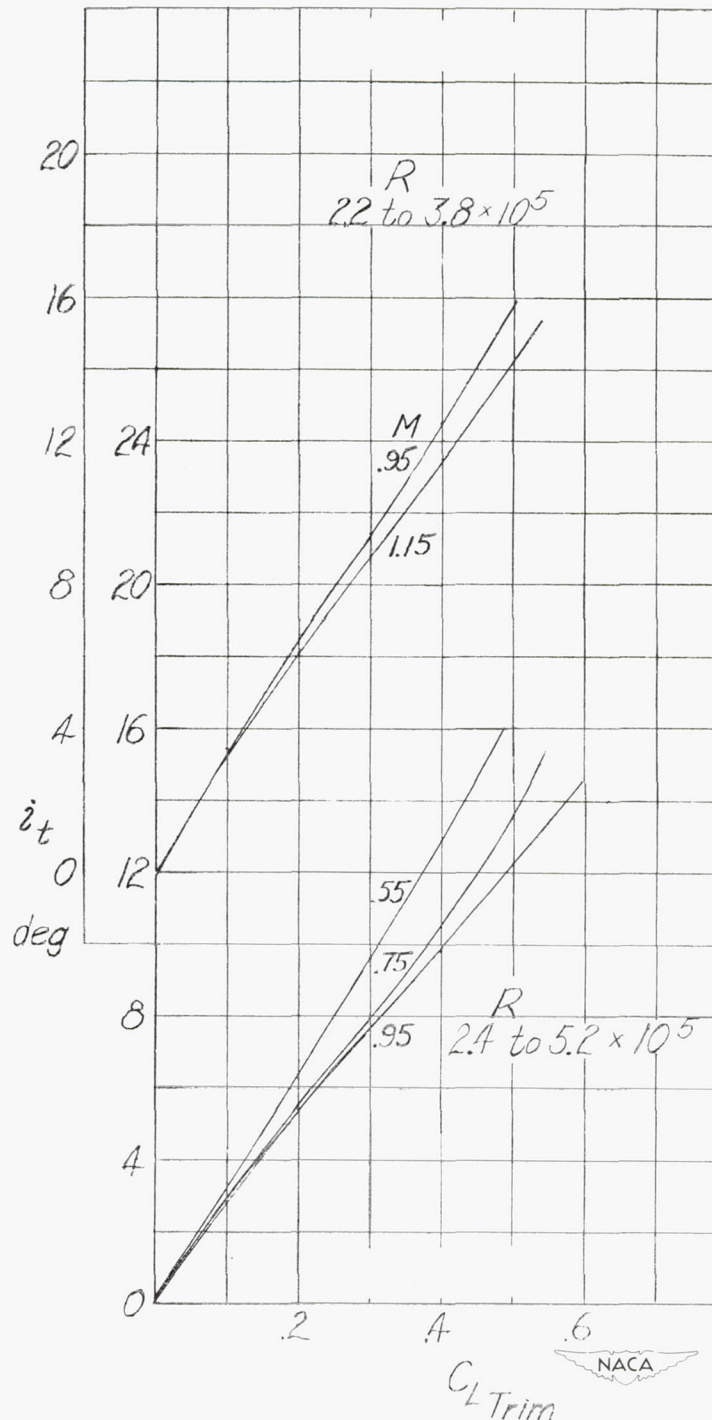
(a) Center of gravity at 40 percent  $\bar{c}$ .

Figure 14.— Calculated variation of stabilizer incidence required for longitudinal trim with trimmed lift coefficient, canard airplane configuration.



(b) Center of gravity at -80 percent  $\bar{c}$ .

Figure 14.- Concluded.

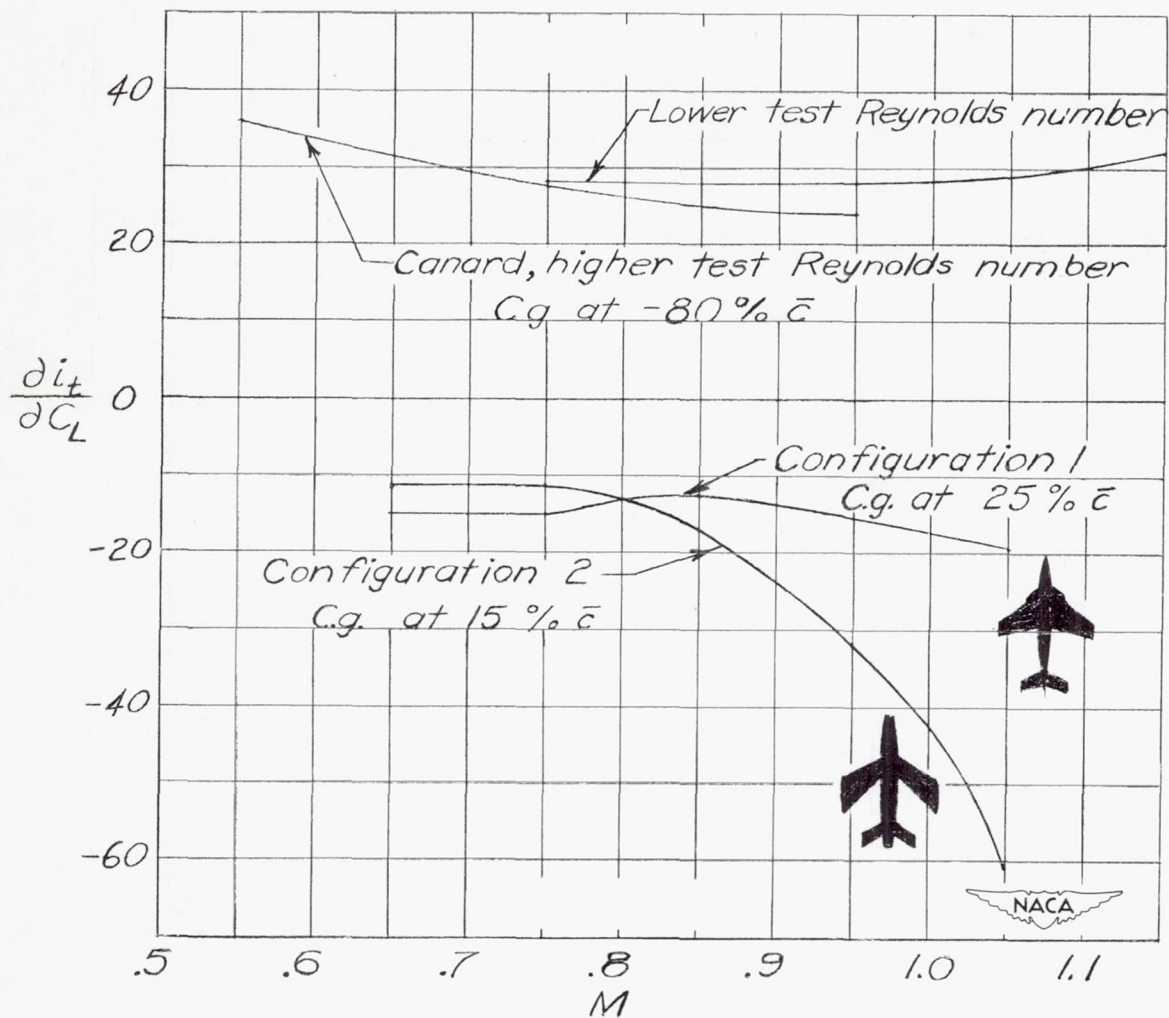
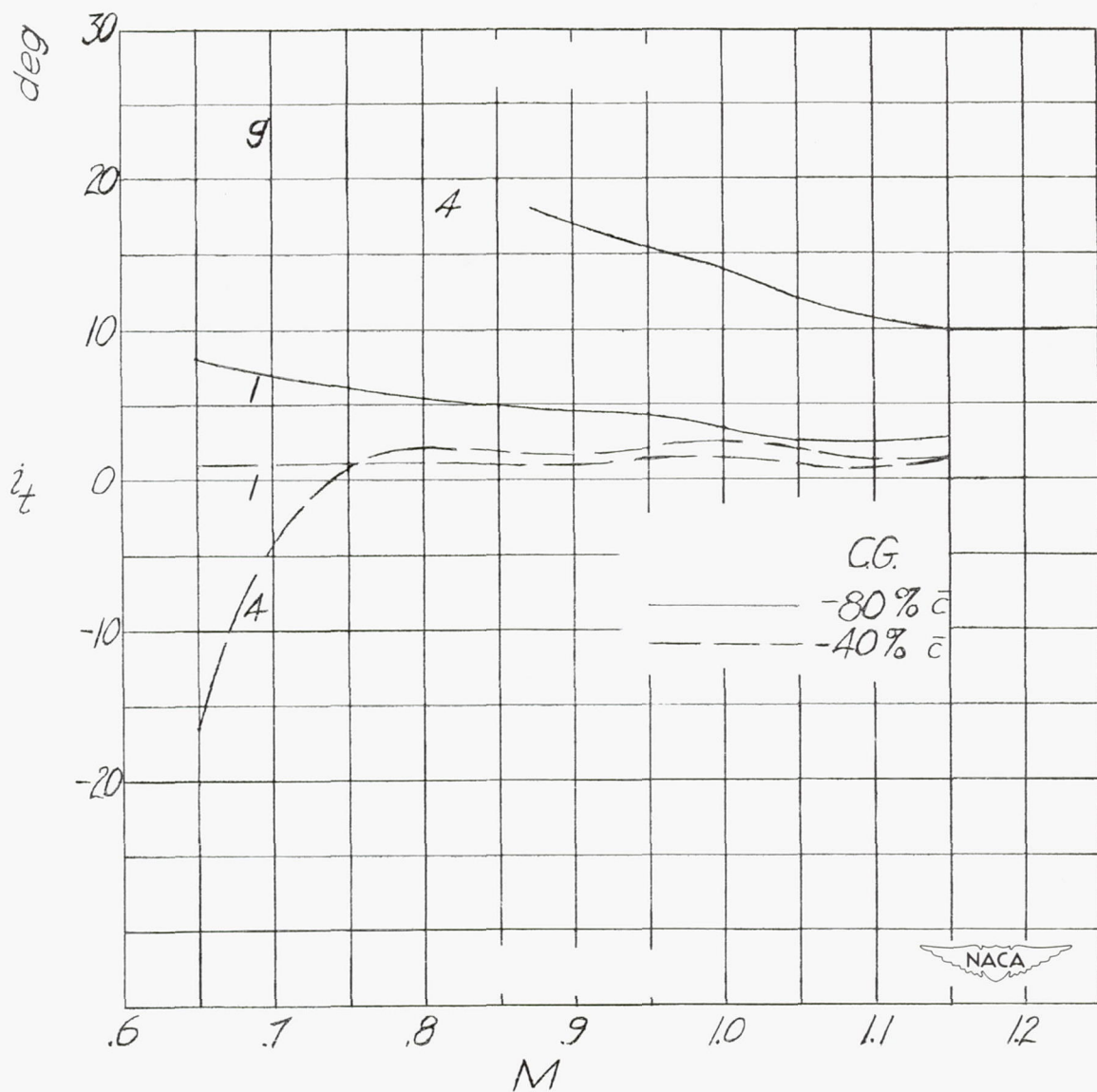
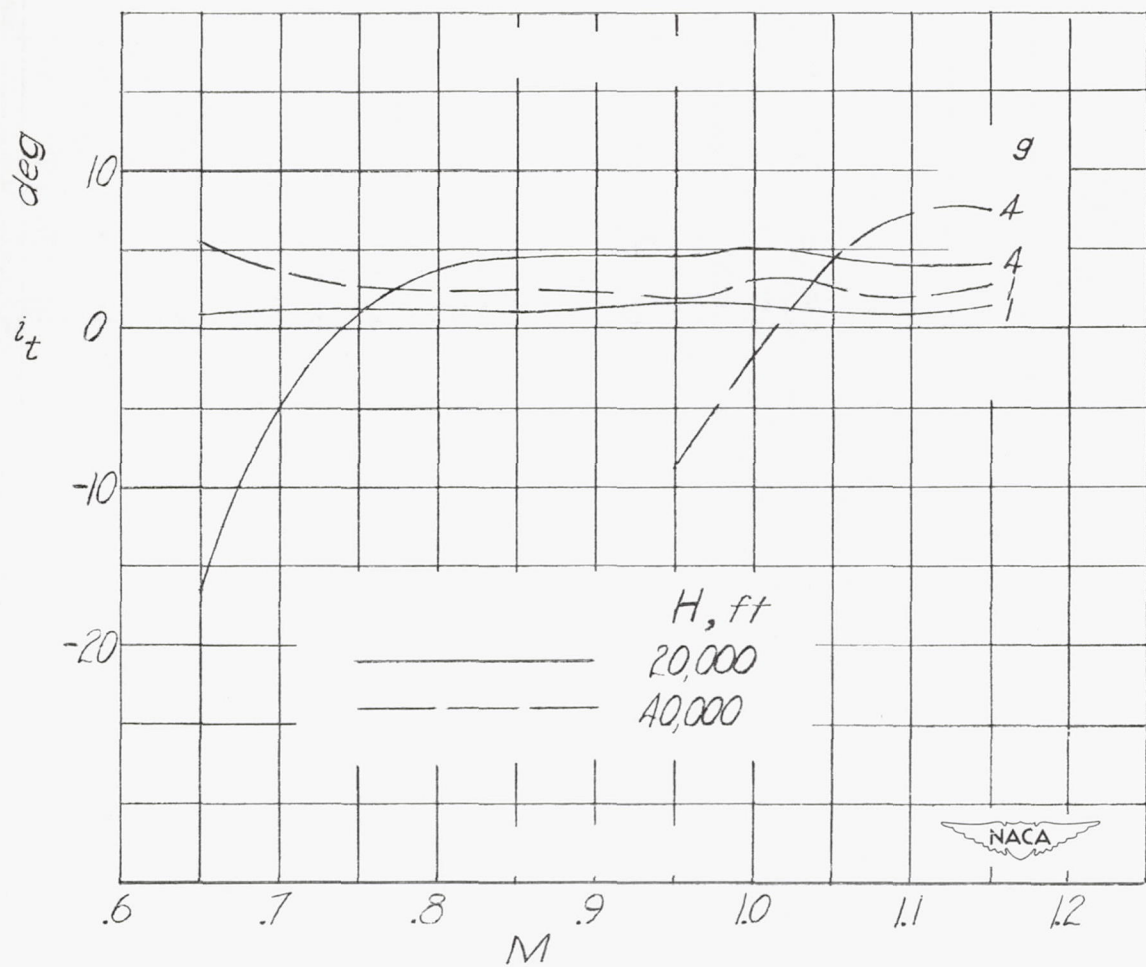


Figure 15.— Variation with Mach number of the calculated stabilizer incidence required per unit change in lift coefficient for the canard and two  $35^\circ$  sweptback conventional airplane configurations.



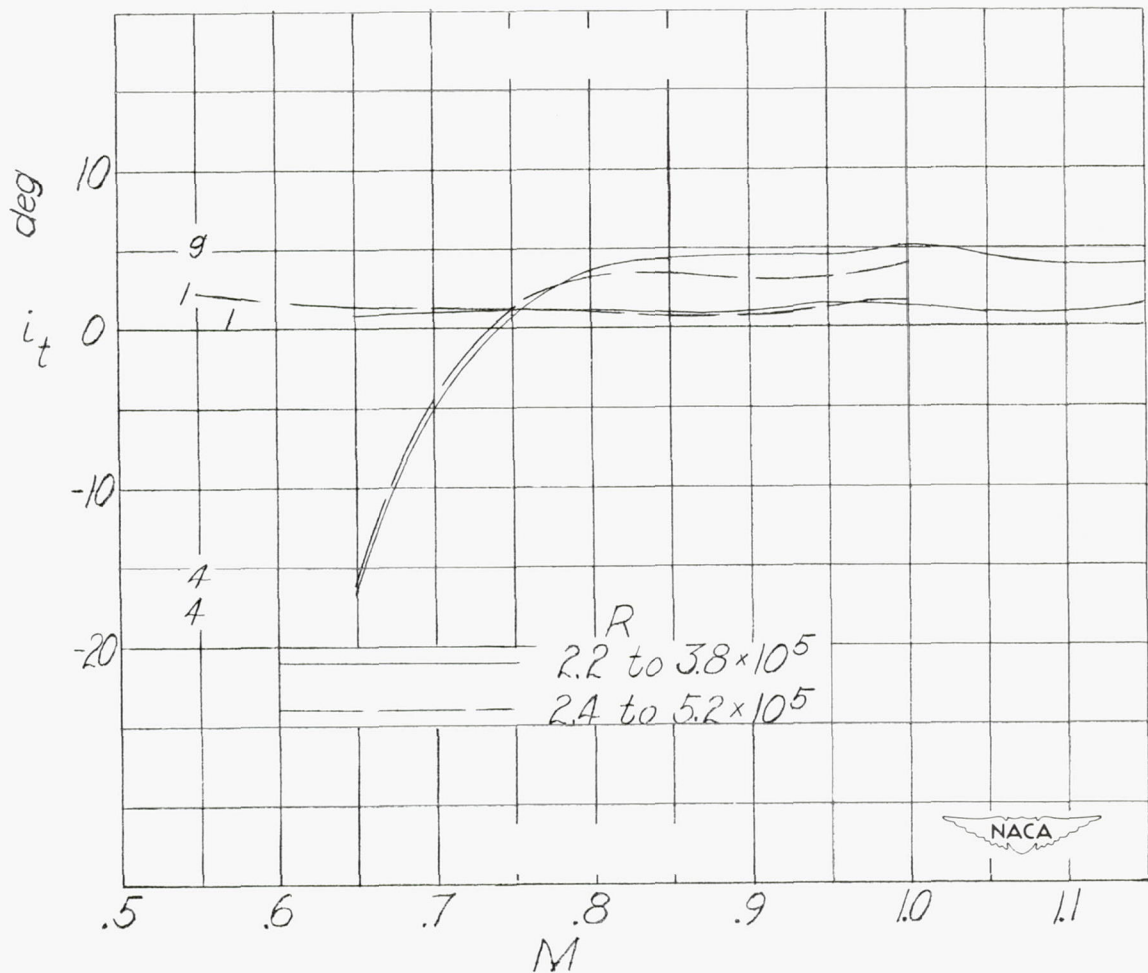
(a) Two center-of-gravity positions, at 20,000 feet, Reynolds number 2.2 to  $3.8 \times 10^5$ .

Figure 16.— Variation of stabilizer incidence for trim with Mach number; canard airplane configuration at a wing loading of 75 lb/sq ft.



(b) Two altitudes, center of gravity at 40 percent  $\bar{c}$ , Reynolds number 2.2 to  $3.8 \times 10^5$ .

Figure 16.—Continued.



(c) Two Reynolds number ranges, center of gravity at  $\frac{1}{4}$ 0 percent  $c$ , at 20,000 feet.

Figure 16.— Concluded.

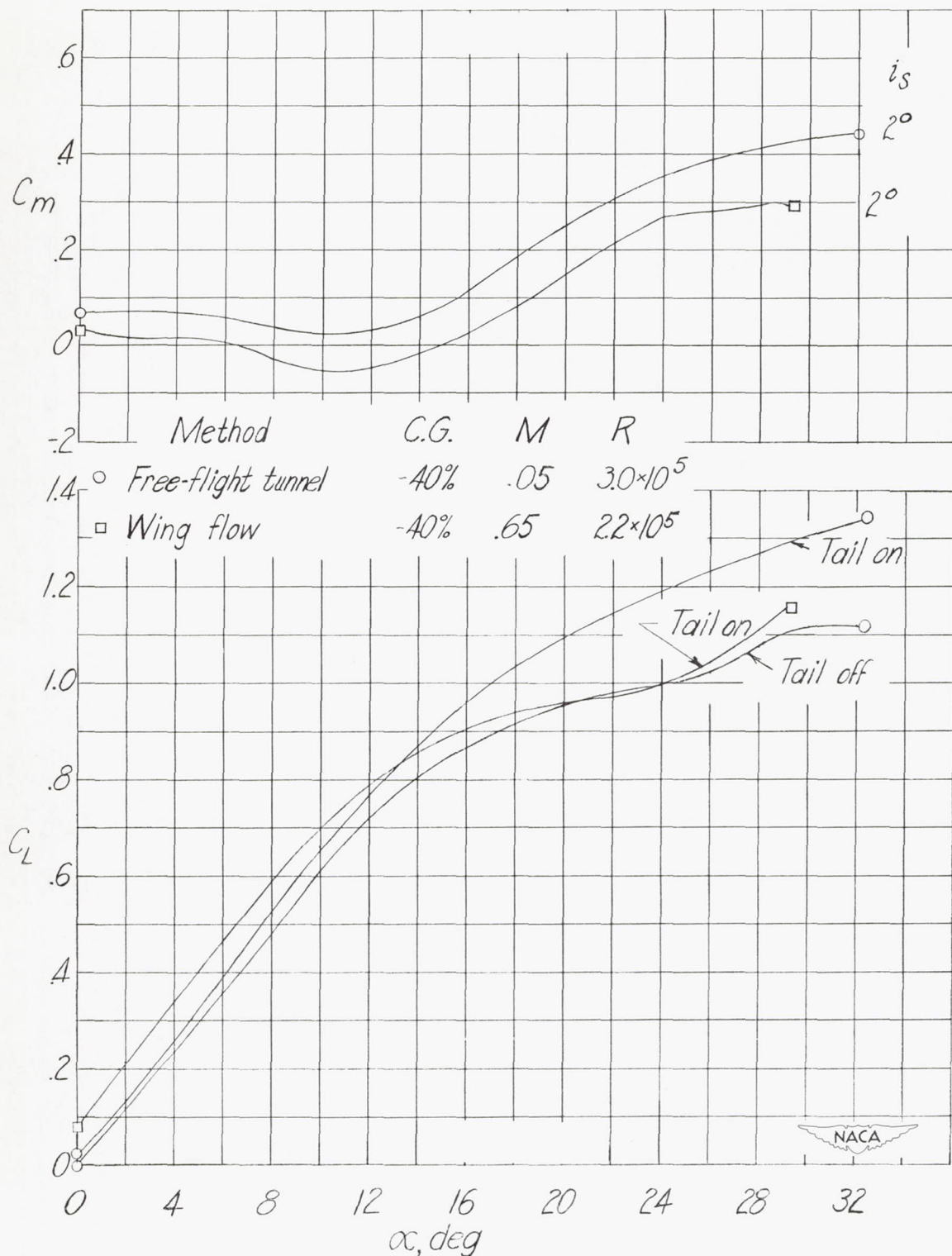


Figure 17.— Comparison of wing-flow data for the canard airplane configuration with unpublished data from the Langley free-flight tunnel.